Quantum criticality in the spin-isotropic pseudogap Bose-Fermi Kondo model: Entropy, scaling, and the *g*-theorem

Zuodong Yu [1,2,*,†] Farzaneh Zamani,[3,*,‡] Pedro Ribeiro,[4,§] and Stefan Kirchner [1,2,∥]

[1]Zhejiang Institute of Modern Physics and Department of Physics, Zhejiang University, Hangzhou, 310027, China
[2]Zhejiang Province Key Laboratory of Quantum Technology and Device, Zhejiang University, Hangzhou 310027, China
[3]Physikalisches Institut and Bethe Center for Theoretical Physics, Universität Bonn, Nussallee 12, D-53115 Bonn, Germany
[4]CeFEMA, Instituto Superior Técnico, Universidade de Lisboa, Av. Rovisco Pais, 1049-001 Lisboa, Portugal

We study the behavior of the entropy of the pseudogap Bose-Fermi Kondo model within a dynamical large-*N* limit, where *N* is related to the symmetry group of the model. This model is a general quantum impurity model that describes a localized level coupled to a fermionic bath having a density of states that vanishes in a power-law fashion near the Fermi energy and to a bosonic bath possessing a power-law spectral density below a cutoff energy. As a function of the couplings to the baths, various quantum phase transitions can occur. We study how the impurity entropy changes across these zero-temperature transitions and compare our results with predictions based on the *g*-theorem. This is accomplished by an analysis of the leading and subleading scaling behaviors. Our analysis shows that the *g*-theorem does not apply to the pseudogap Bose-Fermi Kondo model at the large-*N* level. This inapplicability originates from an anomalous contribution to the scaling function in the hydrodynamic regime where $k_B T > \hbar \omega$ which is absent in the quantum coherent regime, i.e., for $k_B T < \hbar \omega$. We also compare our results with those obtained for the Sachdev-Ye-Kitaev model.

I. INTRODUCTION

Quantum phase transitions (QPTs) have been a central topic of condensed-matter research [1,2]. This is due to a number of reasons. There is, e.g., mounting evidence of a close link between unconventional superconductivity as observed in the cuprates, iron selenides, or 4*f*-based heavy-electron compounds and the occurrence of the so-called strange metal behavior at elevated temperatures in these superconductors. This strange metal phase is characterized by a linear-in-temperature relaxation rate and a logarithmically [in temperature (*T*)] increasing specific heat [3,4]. Moreover, aforementioned unconventional superconductivity is commonly found at the border of magnetism. This observation has led to the speculation that the strange metal out of which superconductivity emerges is caused by a quantum critical point (QCP) hidden under the superconducting dome. There is also an increasing amount of evidence that quantum criticality in strongly correlated metals defies a description in terms of an order-parameter functional [5,6]. Moreover, at least for rare-earth-based intermetallics it has been demonstrated that the general phase diagram of this materials class can be organized around the different possible QCPs [7–10].

QPTs are phase transitions that take place at zero *T* and that can be accessed through some control parameter like pressure, chemical doping, or magnetic field. In contrast to classical phase transitions which occur at nonzero *T* and are driven by the competition of internal energy and entropy, QPTs are a ground-state property. The *T* = 0 entropy is tied to the ground-state degeneracy, which is expected to vanish as required by the third law of thermodynamics. An increase of the entropy at finite *T* in the vicinity of a continuous QPT may, however, still be expected due to the competition of the phases that brings about the QCP. This in turn may promote the emergence of novel order, e.g., superconductivity, in order to avoid the accumulation of entropy associated with proximity to the QCP. A situation that appears to be realized in CeRhIn$_5$, a heavy-electron compound, where a QCP with critical Kondo destruction is hidden beneath the superconducting dome [11]. CeCu$_{6-x}$Au$_x$ is a rare-earth intermetallic compound that undergoes a Kondo-destroying QPT at $x \approx 0.1$ which separates a magnetic from a Kondo-screened paramagnetic phase. The multidimensional entropy landscape of CeCu$_{6-x}$Au$_x$ above the QCP and its relation to quantum critical fluctuations has recently been mapped out [12] which demonstrated a direct link between quantum criticality and the entropy accumulation at finite *T* near the QCP. Such entropy accumulation in the vicinity of quantum criticality may form the basis for dedicated cooling devices in terms of adiabatic processes across the critical coupling [13].

In generic bulk systems, one expects the residual (*T* = 0) entropy to vanish identically in accordance with the third law of thermodynamics. The situation is different in quantum impurity systems which may possess intermediate coupling fixed points that are characterized by a finite residual entropy. Quantum impurity models capture the interplay between a

———————

*These authors contributed equally to this work.

†richzyu@gmail.com

‡zamani@physik.uni-bonn.de

§pedrojgribeiro@tecnico.ulisboa.pt

∥stefan.kirchner@correlated-matter.com

local and discrete quantum mechanical degree of freedom, e.g., a magnetic moment, that hybridizes with a continuous and gapless bath of fermionic or bosonic modes and thus forms an important testing ground for understanding that interplay. A well-known example is the isotropic two-channel Kondo model which possesses a residual entropy $\sqrt{2}$ which is understood in terms of a Majorana zero mode [14–16]. Here, this impurity entropy is defined as the difference between the entropies of the full quantum impurity model and that of the gapless host in which the impurity is embedded, i.e., the bath. As such, it is per se not bound by thermodynamic requirements and could, e.g., even increase as T decreases. The impurity entropy S can in principle be measured in systems with sufficiently low concentrations of quantum impurities, such that contributions to S beyond the lowest, nontrivial order in the concentration can be ignored.

In this paper, we address the behavior of the impurity entropy of a class of quantum impurity systems that feature critical Kondo destruction. Among the simplest quantum impurity system that can undergo a Kondo-destroying QPT is the pseudogap Kondo model [17]. In this model, a QCP separates a Kondo-screened local Fermi-liquid phase from a phase where the local moment remains unquenched down to $T = 0$. The critical properties of this model have been studied extensively using numerical and other renormalization group approaches [18–20], as well as, e.g., dynamical large-N [21], local moment [22,23], and Monte Carlo methods [24,25]. Physical realizations of this model include certain quantum dot structures [26] and disordered metals containing containing low concentrations of magnetic moments [27].

II. MODELS OF CRITICAL KONDO DESTRUCTION

The Bose-Fermi Kondo model (BFKM) is a quantum impurity model that has been introduced in the context of Kondo-destroying quantum criticality which occurs in certain rare-earth-based heavy-electron intermetallics like, e.g., $CeRhIn_5$, $CeCu_{6-x}Au_x$, or $YbRh_2Si_2$ [5,28,29] (see also [30]). Kondo-destroying quantum criticality has been attracting considerable interest as it defies a description in terms of an order-parameter functional [5,6,9,10,31]. This is most clearly reflected in the Fermi volume jump observed in $YbRh_2Si_2$ and from thermodynamic and transport properties at finite T above the QCP and which are indicating a linear-in-T relaxation rate [32–34]. This linear-in-T relaxation rate has been interpreted in terms of ω/T-scaling of the magnetic response as, e.g., observed in $CeCu_{6-x}Au_x$. More recently, ω/T-scaling in the charge response of $YbRh_2Si_2$ has been detected in the vicinity of the magnetic QCP [35]. As nontrivial ω/T-scaling is not expected within the standard Landau-Ginzburg framework for magnetic criticality [1,36], it can serve as a diagnostic tool for unconventional criticality. It has been demonstrated that the spin-isotropic BFKM displays ω/T-scaling at its Kondo-destroying QCP [37,38]. In the BFKM, Kondo screening becomes critical due to the competition with a singular bosonic bath. Its properties have been investigated using a range of methods. The large-N limit of the BFKM has been considered in Ref. [37] while renormalization group (RG) methods have been used in Refs. [39,40]. The model has also been addressed using numerical renormalization

group (NRG) generalizations to include bosons [41,42]. The spin-anisotropic BFKM includes the spin-boson model as a limiting case. The BFKM arises within the extended dynamical mean field or EDMFT approach to quantum criticality in rare-earth intermetallics which maps the Kondo lattice model to a BFKM augmented with a self-consistency condition [5,9]. The model also arises in quantum dot structures attached to ferromagnetic leads [43,44].

In the pseudogap BFKM, gapless bosonic and fermionic baths are coupled to a local moment. The dynamics of this model is described by

$$H_{\text{pgBFKM}} = H_{\text{bath}} + H_{\text{b−s}}, \tag{1}$$

$$H_{\text{bath}} = \sum_{k,\sigma} \varepsilon_k c_{k,\sigma}^\dagger c_{k,\sigma} + \sum_q \omega_q \vec{\phi}_q^\dagger \vec{\phi}_q,$$

$$\begin{aligned} H_{\text{b−s}} &= J_K^\parallel S^z s_c^z + \frac{J_K^\perp}{2}(S^+ s_c^- + S^- s_c^+) \\ &\quad + g^\parallel S^z(\phi_0^{z,\dagger} + \phi_0^z) + g^\perp \sum_{i=x,y} S^i(\phi_0^{i,\dagger} + \phi_0^i), \end{aligned}$$

$$\tag{2}$$

where H_{bath} denotes the bath part and $H_{\text{b−s}}$ describes the coupling between bath and impurity degrees of freedom. $J_K^\perp$ and $J_K^\parallel$ are the transversal and longitudinal Kondo exchange coupling constants between the local moment $\boldsymbol{S}$ and the spin density of the fermionic bath at the impurity location, given by $s_c^z = \sum_{k,k'}(c_{k\uparrow}^\dagger c_{k'\uparrow} - c_{k\downarrow}^\dagger c_{k'\downarrow})$, $s_c^+ = \sum_k c_{k\uparrow}^\dagger c_{k\downarrow}$, and $s^- = (s^+)^\dagger$. $g^\perp$ and $g^\parallel$ are the transversal and longitudinal couplings between the local moment and the bosonic bath, and ω_q (ε_k) is the bosonic (fermionic) bath dispersion. The pseudogap density of states (DOS) of the fermionic bath is characterized by a power-law dependence as the Fermi energy ($\varepsilon_F = 0$) is approached, i.e., $\sum_k \delta(\omega - \varepsilon_k) \sim |\omega|^r \Theta(D - |\omega|)$, while the bosonic spectral density is characterized by a sub-Ohmic behavior at low energies, i.e., $\sum_q[\delta(\omega - \omega_q) - \delta(\omega + \omega_q)] \sim |\omega|^{1-\epsilon}\text{sgn}(\omega)\Theta(\Lambda - |\omega|)$.

The pseudogap BFKM model contains as special cases the pure pseudogap Kondo model ($g^\perp = g^\parallel = 0$) and the Bose Kondo model ($r = 0$). Each of the two allow to critically destroy Kondo screening either through the depletion of fermionic screening states or via the coupling to a singular bosonic bath that can compete with spin-flip scattering between fermionic bath and local moment. The combination of the two possibilities of Kondo screening suppression in the pseudogap BFKM thus allows to study the interplay of both effects near critical Kondo destruction. As a result, the general phase diagram of this model is correspondingly rich. So far, it has been studied using perturbative RG in the spin-isotropic case, e.g., for $g^\perp = g^\parallel$ and $J_K^\perp = J_K^\parallel$ [45,46] and in the easy-axis case ($g^\perp = 0$ and $J_K^\perp = J_K^\parallel$) using NRG [47,48], and continuous-time quantum Monte Carlo (CT-QMC) methods [48,49]. Here, we will study the SU(2)-symmetric pseudogap BFKM in a dynamical large-N limit, where the SU(2) symmetry group is enlarged to SU(N).

The dynamical large-N method is not capable of capturing the local Fermi-liquid fixed point and instead results in an intermediate coupling fixed point that corresponds to

an overscreened multichannel Kondo ground state possessing non-Fermi-liquid properties [50,51]. This shortcoming notwithstanding, the large-N method yields controlled results for the critical properties of the pseudogap Kondo model and sub-Ohmic BFKM that are in line with those obtained using NRG and CT-QMC [24,38,52].

In quantum impurity models with a bulk component that is conformally invariant, a conformal mapping can be found to obtain boundary correlators at temperatures $T > 0$ from their $T = 0$ counterparts [53,54]. A two-point correlator of a primary conformal field Φ with scaling dimension Δ exhibits at $T = 0$ a power-law decay $\langle \Phi(\tau, T = 0) \Phi(0, T = 0) \rangle \sim \tau^{-2\Delta}$. This gives rise to a scaling form [55]

$$\chi_{\Phi\Phi}(\tau, T) \equiv \langle \Phi(\tau, T) \Phi(0, T) \rangle \sim \left(\frac{\pi T}{\sin(\pi \tau T)} \right)^{2\Delta} \quad (3)$$

at $T \neq 0$. The Fourier transform of Eq. (3) implies an ω/T-scaling form of $\chi_{\Phi\Phi}(\omega, T)$, provided $0 < 2\Delta < 1$ (see Appendix D). For the boundary entropy of conformally invariant systems, a relation known as the g-theorem exists, linking the boundary contribution to the fixed-point entropy with the renormalization group (RG) flow [53]. According to this theorem, the boundary entropy decreases along RG trajectories. A proof of the g-theorem has been provided in Ref. [56].

The pseudogap BFKM does not possess conformal invariance. Both the pseudogap DOS of the fermionic bath and the sub-Ohmic spectral density of the bosonic bath break conformal invariance. Interestingly, a scaling behavior as in Eq. (3) for $\tau \to \beta/2$ at sufficiently large β has been reported to emerge near quantum criticality in a range of models which can be viewed as special cases of the pseudgap BFKM [24,25,38,57].

The emergence of the scaling form (3) is confined to the scaling regime of the associated QCP and does in itself not imply the applicability of the g-theorem. It is thus not *a priori* clear if it is at all possible to relate the boundary entropy to the RG flow. In this paper, we are primarily concerned with the fate of the g-theorem of the pseudogap BFKM in the so-called large-N limit specified below. In contrast to earlier results [46], we find that the g-theorem is not fulfilled in the pseudogap BFKM model. We benchmark our approach against the pure Kondo model which is conformally invariant as well as against the so-called Sachdev-Ye-Kitaev (SYK) model in the large-N limit.

In the following, we introduce the Hamiltonian of the pseudogap BFKM in Secs. III and IV discusses the dynamical large-N limit and the evaluation of the impurity entropy. In Sec. V, we present our results for the scaling function in ω and τ and the boundary entropy at the various fixed points. This leads us to conclude that in the pseudogap BFKM the boundary entropy does not always decrease along the RG flow. We trace back this breakdown of the g-theorem to an anomalous contribution to the τT-scaling function present at all intermediate fixed points. A summary recapitulates our findings and puts them in perspective. Appendices A–F contain supplementary results and details.
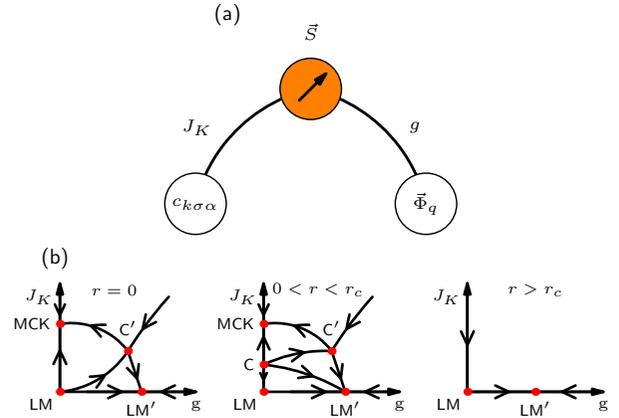

FIG. 1. (a) Sketch of the BFKM. (b) Flow diagram for different values of r and $0 \leqslant \epsilon \leqslant 1$. For the case considered in this paper ($\kappa = M/N = \frac{1}{2}$) one finds $r_c \approx 0.3115$. For details, see main text.

III. SU(N) × SU(M) MODEL

We study the large-N version of the multichannel BFKM, featuring a quantum spin (S) coupled to gapless fermionic (c) and bosonic (Φ) excitations, as illustrated in Fig. 1(a). In the large-N version of the model the SU(2) degree of freedom is generalized to SU(N) and the fermionic fields transform under the fundamental representation of SU(N) × SU(M), where M represents the number of degenerate charge channels of the fermionic bath. Likewise, the N-component bosonic vector fields transform under SU(N). The system is thus described by the Hamiltonian

$$H = \sum_{k\sigma\alpha} \varepsilon_k c_{k\sigma\alpha}^\dagger c_{k\sigma\alpha} + \sum_q \omega_q \Phi_q^\dagger \Phi_q$$
$$+ \frac{J_K}{N} S s_c + \frac{g}{\sqrt{N}} \sum_q S(\Phi_q^\dagger + \Phi_q), \quad (4)$$

where σ and α are, respectively, the SU(N)-spin and SU(M)-channel indices and p, q are momentum indices. The total c-electron spin-density at the impurity site is

$$s_c^i = \sum_{\alpha,\sigma,\sigma'} \sum_{p,p'} c_{p\sigma\alpha}^\dagger t_{\sigma,\sigma'}^i c_{p'\sigma'\alpha}. \quad (5)$$

In this equation, the generators of su(N) in the fundamental representation are referred to as t^i ($i = 1, \ldots, N^2 - 1$). The large-N limit is taken in such a way that the ratio $\kappa = M/N$ is kept fixed while $N \to \infty$ and $M \to \infty$. Note that the fermionic and bosonic baths are fully characterized by their local spectral properties. For the fermions we consider a density of states (DOS) of the form

$$A_c(\omega) = A_0 \theta(D - |\omega|)|\omega|^r, \quad (6)$$

where D is a high-energy cutoff. A_0 is fixed through $\int d\omega A_c(\omega) = 1$. In what follows, we focus on $r \in [0, 1[$. The pseudogap Kondo model with negative r has, e.g., been studied in Refs. [58,59]. The bosonic spectral density is taken to be of the form

$$A_\Phi(\omega) = A_{\Phi_0} \text{sign}(\omega) \theta(\Lambda - |\omega|)|\omega|^{1-\epsilon}, \quad (7)$$

where Λ is a high-energy cutoff, $\epsilon \in [0, 1[$ character-izes the sub-Ohmic DOS, and A_{Φ_0} is chosen such that $\int_0^{\Lambda} d\omega A_{\Phi_0}(\omega) = 1$.

At $T = 0$, the phase space of the pseudogap BFKM encom-passes a number of fixed points. The nature of the fixed points and the structure of the flow diagram depend on the values of r and ϵ. For $0 < r < 1$ and $0 \leqslant \epsilon < 1$ there are three cases that need to be distinguished [see Fig. 1(b)].

For $r = 0$, the standard Bose-Fermi Kondo model is ob-tained [5,39]. Its large-N version possesses an over-screened multichannel Kondo phase (MCK) at small g/J which is separated from a critical local moment phase, controlled by (LM'), by an unstable critical point (C') that features critical Kondo destruction [37]. The unstable trivial fixed point (LM) corresponds to the fully decoupled impurity.

In the presence of a pseudogap, i.e., $r > 0$, the suppression of the electronic DOS at the Fermi energy makes the MCK fixed point less stable and leads to the appearance of a further critical point (C). Beyond a critical value of r, i.e., $r > r_c$, the suppression of the electronic DOS is so effective that the MCK fixed point disappears leading to a phase diagram where LM' is the only stable fixed point. Note that the standard Kondo problem corresponds to $M = 1$ and $N = 2$. In this exactly screened case, the MCK gives way to single-channel Kondo physics which is governed by a strong coupling fixed point ($J_K \to \infty$) and displays Fermi-liquid signatures. Within the large-N description adopted in this paper, this strong cou-pling fixed point is out of reach.

The characterization of each phase and the scaling laws for the different quantities were obtained in [37–39] both by perturbative RG and large-N methods. In particular, it was found that the $T = 0$ scaling properties in the characteristic quantum critical fan are in line with dynamical ω/T-scaling (see below) [2,37,39].

IV. METHODS

A. Dynamical large N

We resort to a pseudofermion representation of the local spin, i.e., $S^i = \sum_{\sigma\sigma'} f_\sigma^\dagger \tau_{\sigma,\sigma'}^i f_{\sigma'}$. Here, $\tau^i (i = 1, \ldots, N^2 - 1)$ forms an antisymmetric representation of su(N) fixed by imposing the constraint $Q = \sum_\sigma f_\sigma^\dagger f_\sigma = qN$. A dynamical Lagrange multiplier λ enforces the constraint within the func-tional integral formalism. We have chosen $q = \frac{1}{2}$ in this work.

The imaginary-time action for the pseudogap BFKM (4) is given by

$$
S^{\mathrm{DLN}} = -\int_\tau \left(c_{k\alpha\sigma}^\dagger g_c^{-1} c_{k'\alpha\sigma} + \Phi_q^\dagger g_\Phi^{-1} \Phi_q + f_\sigma^\dagger g_f^{-1} f_\sigma \right)
$$
$$
+ \int_\tau \left[\frac{J_K}{N} f_\sigma^\dagger f_{\sigma'} c_{k\sigma'\alpha}^\dagger c_{k'\sigma\alpha} - \lambda q_0 N \right.
$$
$$
\left. + \frac{g}{\sqrt{N}} f_\sigma^\dagger f_{\sigma'} \tau_{\sigma\sigma'}^i \left(\Phi_q^{i\dagger} + \Phi_q^i \right) \right], \tag{8}
$$

with $g_c(i\omega_n) = (i\omega_n - \epsilon_k)^{-1}$ and $g_\Phi(i\nu_n) = (i\nu_n - \omega_q)^{-1}$ are, respectively, the fermionic and bosonic degrees of freedom of the bath modes where $i\omega_n = 2\pi i(n + 1/2)/\beta$ and $i\nu_n =$

$2\pi i n/\beta$, $n \in \mathbb{Z}$ are the fermionic and bosonic Matsubara fre-quencies. The bare pseudofermion Green's function is defined as $g_f(i\omega_n) = (i\omega_n - \lambda)^{-1}$.

In the following, we employ a dynamical large-N pro-cedure [21,37,50,60] briefly described in Appendix A and summarized below for convenience. The procedure consists of introducing a bosonic Hubbard-Stratonovich field B to decou-ple the fermionic interacting term. This allows us to integrate out the bath degrees of freedom and to recover an action solely in terms of local fields. The interacting terms in the action are subsequently decoupled with the help of two sets of bilocal fields W and Q.

For the impurity contribution to the free energy $N f^{\mathrm{DLN}}$ associated with Eq. (8), we write $f_{\mathrm{imp}} = f^{\mathrm{DLN}} - f_{\mathrm{bulk}}$, where f_{bulk} denotes the bath contribution defined as the free energy associated with H_{bath} [Eq. (4)] for $J_K = 0 = g$. As shown in Appendix A, the impurity contribution of Eq. (8) can be written as

$$
f_{\mathrm{imp}} = \int_\tau [\bar{Q}(\tau)Q(-\tau) + \bar{W}(-\tau)W(\tau) - q_0\lambda(\tau)]
$$
$$
+ T\kappa \mathrm{Tr} \ln \left(-G_B^{-1} \right) - T\mathrm{Tr} \ln \left(-G_f^{-1} \right), \tag{9}
$$

where $G_B^{-1} = g_B^{-1} - \Sigma_B$ and $G_f^{-1} = g_f^{-1} - \Sigma_f$ and

$$
\Sigma_B(\tau) = -g_c(-\tau)Q(\tau),
$$
$$
\Sigma_f(\tau) = \bar{Q}(\tau) + g\bar{W}(\tau) + g g_\Phi(\tau)W(\tau). \tag{10}
$$

Note that the definition of the Hubbard-Stratonovich fields is slightly different to that used in Refs. [24,37,50,60]. As shown below, this change in the Hubbard-Stratonovich fields does not affect the self-energy values at the saddle point but is more convenient in the present context. The decoupling scheme chosen here avoids the generation of a temperature-dependent Jacobian, related to $g_c(\tau)$ and $g_\Phi(\tau)$, which would need to be properly taken into account when evaluating the impurity en-tropy. Formally, both definitions of the Hubbard-Stratonovich fields are equivalent and lead to identical values for the self-energies and impurity entropy but the choice adopted here is more convenient when explicitly evaluating the temperature dependence of the impurity entropy.

The partition function in Eq. (9) is suitable for a saddle-point approximation

$$
\frac{\delta f_{\mathrm{imp}}}{\delta X} = 0, \tag{11}
$$

where X represents $\bar{Q}, Q, \bar{W}, W, \lambda$. The propagators for f and B are determined by the saddle-point equations which relate proper self-energy contributions to the bilocal fields. In the limit of $N, M \to \infty$ (while κ is kept constant), the saddle-point approximation

$$
Q(\tau) = -G_f(\tau), \tag{12}
$$
$$
\bar{Q}(\tau) = -\kappa G_B(\tau)g_c(\tau), \tag{13}
$$
$$
W(\tau) = -gG_f(\tau), \tag{14}
$$
$$
\bar{W}(\tau) = -gG_f(\tau)g_\Phi(-\tau) \tag{15}
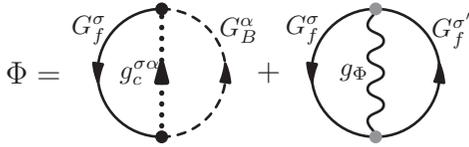$$

becomes exact [21,37,50,60].

FIG. 2. Leading-order contribution. Each vertex contains factor of $\sqrt{\frac{1}{N}}$. Summation is assumed for all σ, α which makes the diagram order N.

This procedure yields the following self-consistency equations (for details, see Appendix A):

$$\Sigma_f(\tau) = \Sigma_f^1(\tau) + \Sigma_f^2(\tau) \tag{16}$$
$$= -\kappa G_B(\tau) g_c(\tau) - g^2 G_f(\tau) \tilde{g}_\Phi(\tau),$$
$$\Sigma_B(\tau) = G_f(\tau) g_c(-\tau) \tag{17}$$

with $\tilde{g}_\Phi(\tau) = g_\Phi(\tau) + g_\Phi(-\tau)$. This redefinition is equivalent to extending the sum over q from positive ω_q to negative values with $\omega_{-q} = -\omega_q$. The local spin susceptibility at the saddle point is given in terms of the pseudoparticle propagator G_f as

$$\chi(\tau) = G_f(\tau) G_f(-\tau) \tag{18}$$

while the local t-matrix is obtained as the convolution of $G_f(\omega, T)$ and $G_B(\omega, T)$ from

$$\mathcal{T}(\tau) = G_f(\tau) G_B(-\tau). \tag{19}$$

At the saddle point, the free energy is given by

$$f_{\text{imp}} = \int_\tau [\kappa G_B(\tau) g_c(\tau) G_f(\tau) + g^2 G_f(-\tau) g_\Phi(\tau) G_f(\tau)]$$
$$+ T\kappa \text{Tr} \ln\left(-G_B^{-1}\right) - T\text{Tr}\ln\left(-G_f^{-1}\right) - \lambda q_0 \tag{20}$$

and f_{imp} naturally assumes the form

$$f_{\text{imp}} = \Phi[G_f, G_B, \lambda] - T\,\text{Tr} G_f \Sigma_f + T\kappa\,\text{Tr} G_B \Sigma_B$$
$$+ T\kappa\,\text{Tr} \ln\left(-G_B^{-1}\right) - T\,\text{Tr}\ln\left(-G_f^{-1}\right) - \lambda q_0. \tag{21}$$

Recognizing Φ as the Legendre transform of f_{imp}, the stationary condition in Eq. (11) translates to

$$\frac{\delta \Phi}{\delta G_a} = \eta_a \Sigma_a \ (a = f, B), \tag{22}$$

where $\eta_f = 1$ and $\eta_B = -1$. Equation (22) identifies Φ, depicted in Fig. 2, as the corresponding Luttinger-Ward functional. Our derivation shows that a rigorous large-N limit is equivalent to a conserving approximation in the Kadanoff-Baym sense [61–63] (see also Appendix C). Identifying Luttinger-Ward functionals through associated saddle-point limits is one way of constructing such functionals in a nonperturbative manner [64].

The relation between G_a and Σ_a is given by the Dyson equation $G_a^{-1} = g_a^{-1} - \Sigma_a$, with $a = B, f$ and where the bare propagators are given by $g_B = -J_K$ and $g_f = \frac{1}{i\omega - \lambda}$. As B is a Hubbard-Stratonovich decoupling field, its bare part only depends on the coupling constant and any dynamics has to be acquired through interaction effects. In addition to Eqs. (16) and (17), G_f has to respect the constraint $G_f(\tau \to 0^-) = q_0$, which is enforced through the Lagrange multiplier λ. For the

relation between the free energy and the saddle-point action S one finds $f = S/\beta$. From the entropy

$$s_{\text{full}} = -N \frac{df^{\text{DLN}}}{dT} \tag{23}$$

we can split off the impurity contribution, defined by $s_{\text{imp}} = s_{\text{full}} - s_0$, where s_{full} is the total entropy of the system and s_0 is the contribution of the bath in the absence of the impurity. Note that, defined as a difference, s_{imp} does not need to obey the second law of thermodynamics. In the remainder, we will omit the subscript on s_{imp}, i.e., $s = s_{\text{imp}}$. As detailed in Appendix B, we obtain

$$s = -\int \frac{d\omega}{\pi} \left\{ \partial_T n_b(\omega) \kappa \, \text{Im}\left\{ \ln\left[-G_B^{-1}(\omega)\right]\right\} \right.$$
$$+ n_b(\omega)\kappa \, \text{Im}[-G_B(\omega)\partial_T A(\omega)]$$
$$+ \partial_T n_f(\omega) \text{Im}\left\{ \ln\left[-G_f^{-1}(\omega)\right]\right\} \tag{24}$$
$$+ n_f(\omega) \text{Im}[G_f(\omega)\partial_T B(\omega)]$$
$$\left. + \partial_T n_f(\omega) \text{Im}\left[\Sigma_f^1(\omega) G_f(\omega) + \frac{1}{2}\Sigma_f^2(\omega) G_f(\omega)\right] \right\},$$

where the imaginary parts of $\partial_T A(\omega)$ and $\partial_T B(\omega)$ are

$$\text{Im}\,\partial_T A(\omega) = \int \frac{d\omega'}{\pi} G_f''(\omega')$$
$$\times g_c''(\omega' - \omega)\partial_T[n_f(\omega') - n_f(\omega' - \omega)], \tag{25}$$
$$\text{Im}\,\partial_T B(\omega) = \int \frac{d\nu}{\pi} g^2 g_\Phi''(\nu)$$
$$\times G_f''(\omega - \nu)\partial_T[n_f(\nu - \omega) + n_b(\nu)] \tag{26}$$

and the reals parts are obtained through Kramers-Kronig relations.

B. Scaling

Asymptotically exact results for the frequency behavior of G_f and G_B in the $T = 0$ limit can be obtained through a scaling ansatz. Following Parcollet et al. [50], we set

$$G_f(\tau) = -A_1\left(\frac{\tau_0}{\tau}\right)^{\alpha_f} - A_2\left(\frac{\tau_0}{\tau}\right)^{\alpha_f'} + \cdots, \tag{27}$$
$$G_B(\tau) = -B_1\left(\frac{\tau_0}{\tau}\right)^{\alpha_B} - B_2\left(\frac{\tau_0}{\tau}\right)^{\alpha_B'} + \cdots, \tag{28}$$

valid at $T = 0$ and for $\tau \gg \tau_0$, where τ_0 is a short-time cutoff. The real-frequency counterpart of these expressions is obtained via analytic continuation of the Fourier transform as outlined in Appendix D. For $G_a(\tau) = -(\frac{1}{\tau})^{\alpha_a}$ ($a = f$ or $a = B$), one finds in the $T = 0$ limit,

$$G_B(\omega + i0^+, \beta \to \infty) = -\frac{\pi \tau_0^{\alpha_B}}{\Gamma(\alpha_B)} X_{\alpha_B}^B |\omega|^{\alpha_B - 1}, \tag{29}$$
$$G_f(\omega + i0^+, \beta \to \infty) = -\frac{\pi \tau_0^{\alpha_f}}{\Gamma(\alpha_f)} X_{\alpha_f}^f |\omega|^{\alpha_f - 1}, \tag{30}$$

where $X_{\alpha_B}^B = \tan\left(\frac{\pi\alpha_B}{2}\right) + i\,\text{sgn}(\omega)$ and $X_{\alpha_f}^f = -\cot\left(\frac{\pi\alpha_f}{2}\right)\text{sgn}(\omega) + i$ [see (D7) and (D8)].

TABLE I. Scaling exponents of G_B and G_f at the various fixed points.

C	$r + \alpha_f = 1 - \alpha_B$
MCK	$\kappa = \frac{(1-\alpha_f)\tan(\pi\alpha_f/2)}{(r+\alpha_f)\tan(\pi(r+\alpha_f)/2)}$
C'	$\alpha_f = \epsilon/2, \ \alpha_B = 1 - (r + \epsilon/2)$
LM'	$\alpha_f = \epsilon/2, \ \alpha_B = 1 + (r + \epsilon/2)$

Inserting these expressions into the saddle-point equations (12)–(15), one obtains α_f and α_B (see Appendix E). For the special case $r = 0$, similar results have been reported in [37,43]. Our results for α_f and α_B reduce to those of Ref. [21] for the pure pseudogap Kondo model at large N. Moreover, the large-N exponent for the t-matrix of the pseudogap Kondo model at the multichannel Kondo fixed point agrees with that of the SU(2)-symmetric pseudogap Kondo model at its strong coupling fixed point [18,65]. Our results for the leading behavior, i.e., α_f and α_B, are summarized in Table I. From the scaling ansatz for G_f and G_B one also obtains $\chi(\omega) \sim |\omega|^{2\alpha_f - 1}$ and $\mathcal{T}(\omega) \sim |\omega|^{\alpha_f + \alpha_B - 1}$ to leading order.

In the pseudogap BFKM, both fermionic and bosonic baths break conformal symmetry but for $r = 0$ and in the absence of a bosonic bath ($g = 0$), the Hamiltonian possesses conformal symmetry. The resulting invariance can be used to extend the leading-ω behavior scaling ansatz to the leading-T dependence. One obtains

$$G_f(\tau, \beta) = \left(\frac{\tau_0 T}{\sin \pi \tau T}\right)^{\alpha_f} + \cdots \tag{31}$$

and likewise for G_B. The ... in Eq. (31) stand for subleading corrections. This form for G_f and G_B, fully determines low-energy properties, in particular, the fixed-point (or zero-temperature) entropy [50]. Equation (31) implies ω/T-scaling, i.e.,

$$G_f(\omega, T) = T^{\alpha_f - 1}\Phi_f(\omega/T) + \cdots \tag{32}$$

in the scaling regime, provided $\alpha_f < 1$ which is necessary for the Fourier integral to converge [corresponding statements apply to $G_B(\omega, T)$]. It follows from Eqs. (31) and (32) that $G_f(\omega, T = 0) \sim \omega^{\alpha_f - 1}$ and $G_f(\omega = 0, T) \sim T^{\alpha_f - 1}$. The marginal case $\alpha_f = 1$, which is, e.g., relevant for the standard Kondo problem, where the strong coupling fixed point is described by a boundary conformal field theory, requires an extra energy scale in order to regularize the Fourier transform (see Appendix D). This energy scale can be identified with the Kondo temperature T_K. As a result, a somewhat trivial ω/T-scaling ensues in this case in the limit $T \ll T_K$ and $\omega \ll T_K$.

In what follows, we will pay particular attention to the terms represented by the ellipses in Eq. (31). The $T = 0$ form of these subleading terms can be determined from the saddle-point equations in a fashion analogous to the leading behavior (see Appendix E). As far as the extension to $T \neq 0$ is concerned, a form reminiscent of Eq. (32) may apply to the subleading terms as well, albeit with a different scaling exponent $\alpha_f' > \alpha_f$. Even in that case will the sum of leading and subleading terms together not be of the form of Eq. (32). In other words, the subleading terms necessarily break the ω/T-scaling form of Eq. (32).

C. Numerical solutions

A numerical solution of the large-N equations (12)–(17) for given set $\{r, \alpha_\phi, J_K, g, D, \Lambda\}$ of parameters can be obtained iteratively at $T \neq 0$ and all ω. This is accomplished by Fourier transforming the saddle-point equations to Matsubara space followed by analytic continuation to real frequencies. The self-consistent equation for the self-energies follow as

$$\Sigma_f''(\omega) = -\kappa \int_{-\infty}^{+\infty} \frac{dx}{\pi} G_B''(x) g_c''(\omega - x)[n_b(x) + n_f(x - \omega)]$$

$$- 2g^2 \int_{-\infty}^{+\infty} \frac{dx}{\pi} g_\Phi''(x) G_f''(\omega - x)$$

$$\times [n_b(x) + n_f(x - \omega)], \tag{33}$$

$$\Sigma_B''(\nu) = \int_{-\infty}^{+\infty} \frac{dx}{\pi} G_f''(x) g_c''(x - \nu)[n_f(x) - n_f(x - \nu)]. \tag{34}$$

In order to resolve the $T = 0$ power-law divergences of $G_f(\omega, T)$ and $G_B(\omega, T)$, a logarithmically dense energy mesh is used. To improve convergence of the self-consistency problem, a modified Broyden's scheme is employed [66]. In this work, the criterion used for convergence is that the frequency integral over the absolute value of the difference of two solutions of two consecutive iterations has to be less than 10^{-5}. Once convergence has been reached, the impurity entropy $s(T)$, t-matrix $\mathcal{T}(\omega, T)$, and local spin susceptibility $\chi(\omega, T)$ can be obtained from $G_f(\omega, T)$ and $G_B(\omega, T)$.

D. Zero-temperature entropy

As our goal is to test the validity of the g-theorem for the pseudogap BFKM, the fixed-point value of the entropy is required at all fixed points across the phase diagram. The expression in Eq. (24) simplifies in the $T = 0$ limit provided the local Green functions, i.e., G_f and G_B, display ω/T-scaling, in which case the only contribution to the impurity entropy comes from the logarithmic terms in Eq. (24). As will be demonstrated below, the local Green functions indeed obey $G_a(\omega, T) = T^{\alpha_a - 1}\Phi_a(\omega/T)$ ($a = B, f$ in this equation distinguishes between the bosonic and fermionic Green function) at all fixed points except the weak coupling fixed point (LM).

In this case, the leading part of the free energy, for small T, is given by

$$f_{\text{imp}} = \kappa \int_{-\infty}^{0} \frac{d\omega}{\pi} \left[a_B\left(\frac{\omega}{T}\right) - a_B(-\infty) + 2\kappa n_b(-\omega) a_B\left(\frac{\omega}{T}\right) \right]$$

$$+ \int_{-\infty}^{0} \frac{d\omega}{\pi} \left[a_f\left(\frac{\omega}{T}\right) - a_f(-\infty) - 2n_f(-\omega) a_f\left(\frac{\omega}{T}\right) \right], \tag{35}$$

with

$$a_f(\omega/T) = \arctan \frac{G_f'(\omega, T)}{G_f''(\omega, T)},$$

$$a_B(\omega/T) = \arctan \frac{G_B''(\omega, T)}{G_B'(\omega, T)}.$$

In terms of these functions, the $T = 0$ limit of the entropy follows as

$$s = - \int_{-\infty}^{0} \frac{d\tilde{\omega}}{\pi} [\kappa a_B(\tilde{\omega}) - \kappa a_B(-\infty) + 2\kappa n_b(-\tilde{\omega}) a_B(\tilde{\omega})$$
$$+ a_f(\tilde{\omega}) - a_f(-\infty) - 2n_f(-\tilde{\omega}) a_f(\tilde{\omega})], \quad (36)$$

where n_B and n_f are the bosonic and fermionic distribution functions.

V. RESULTS

We now turn to a discussion of the numerical results, obtained from a self-consistent solution of the saddle-point equations (16) and (17) for $T \neq 0$.

A. Green functions

The local Green functions G_B and G_f display power-law behavior at $T = 0$ and low frequency, i.e., $G_{f,B}(\omega, T = 0) \sim \omega^{\alpha_{f,B}-1}$ near the fixed points (C, C′, LM′, MCK). α_B and α_f can be obtained from the scaling ansatz [Eqs. (27) and (28)] and are listed in Table I. In the following we focus on a representative set of κ, r, and ϵ to discuss our results. We choose $\kappa = \frac{1}{2}$, $r = \frac{1}{4}$, and $\epsilon = \frac{2}{5}$ which corresponds to exponents $\alpha_f = (0.052, 0.2, 0.2, 0.338)$ and $\alpha_B = (0.698, 0.55, 1.45, 0.412)$ for fixed points (C, C′, LM′, MCK), respectively. At $T \neq 0$, by transforming Eq. (3) into real frequencies (see Appendix D), one obtains

$$G_f(\omega) = - \left(\frac{2\pi}{\beta} \right)^{\alpha_f - 1} \tau_0^{\alpha_f} B \left[\frac{\alpha_f}{2} - \frac{i\beta\omega}{2\pi}, \frac{\alpha_f}{2} + \frac{i\beta\omega}{2\pi} \right]$$
$$\times \left(-\cot \frac{\pi\alpha_f}{2} \sinh \frac{\beta\omega}{2} + i \cosh \frac{\beta\omega}{2} \right), \quad (37)$$

$$G_B(\omega) = - \left(\frac{2\pi}{\beta} \right)^{\alpha_B - 1} \tau_0^{\alpha_B} B \left[\frac{\alpha_B}{2} - \frac{i\beta\omega}{2\pi}, \frac{\alpha_B}{2} + \frac{i\beta\omega}{2\pi} \right]$$
$$\times \left(\tan \frac{\pi\alpha_B}{2} \cosh \frac{\beta\omega}{2} + i \sinh \frac{\beta\omega}{2} \right), \quad (38)$$

where $B(x, y)$ is the Euler beta function and a numerical prefactor, equivalent to A_1 of Eq. (E1) and B_1 of Eq. (E2) has been set to one. Equations (37) and (38) can be compared with the numerical solution of the saddle-point equations (16) and (17) for $T \neq 0$. First, we establish that the low-T behavior of $G_f(\omega, T)$ and $G_B(\omega, T)$ is in line with the results obtained from the scaling ansatz for $T = 0$ and $\omega \to 0$.

Figure 3 displays $\mathrm{Im}[G_f(\omega, T = 10^{-9}D)]$ and $\mathrm{Im}[G_B(\omega, T = 10^{-9}D)]$ [D is defined in Eq. (6)] near the intermediate coupling fixed points. Evidently, both Green functions display power-law behavior for $\omega > T$ and below some high-energy cutoff T_K^* which can be identified with $\min[\Lambda, T_K^0]$, where T_K^0 is the Kondo temperature associated with the Kondo model with $g = 0$, $r = 0$ and all other parameters left unchanged. It follows from the Kramers-Kronig relation that the real parts of G_f and G_B feature corresponding power-law behavior. Clearly, the numerical results confirm the conclusions drawn from the scaling ansatz.

From the numerical results we can obtain the T behavior of the Green functions G_f and G_B and consequently obtain the
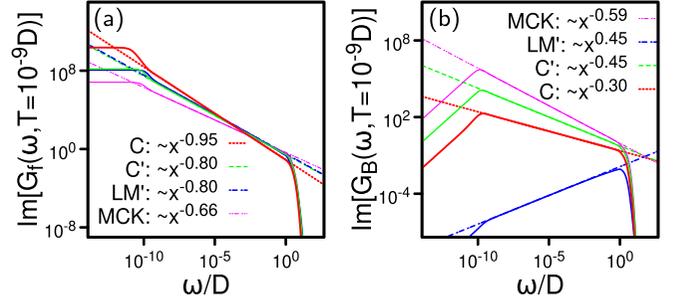

FIG. 3. Numerical results of Green's function with leading power-law fitting at different fixed points. (a) $\mathrm{Im}[G_f(\omega, T = 10^{-9}D)]$, (b) $\mathrm{Im}[G_B(\omega, T = 10^{-9}D)]$.

static susceptibility from $\chi_{\mathrm{stat}}(T) = \mathrm{Re}[\chi(\omega = 0, T)]$. Figure 4(a) shows the T dependence of $G_f(\omega = 0, T)$. Power-law behavior is found in the scaling regime associated with each of the intermediate coupling fixed points. The observed power law in T is compatible with the ω behavior of $G_f(\omega, T = 0)$ and points toward ω/T-scaling. This is indeed observed as shown in Fig. 4(b) for G_f and Fig. 4(c) for G_B near the fixed points C, C′, LM′, and MCK. In each case, we find that the Green function $G_a(\omega, T)$ ($a = f$ or B) obeys

$$G_a(\omega, T) = T^{\alpha_a - 1} \Phi_f(\omega/T) \quad (39)$$

to leading order and with a scaling exponent that agrees within numerical uncertainty with the corresponding exponent from Table I. From the scaling behavior of G_f and G_B one can infer a related scaling for $\mathcal{T}$ and χ. This is explicitly demonstrated in Fig. 5 for the critical point C′.
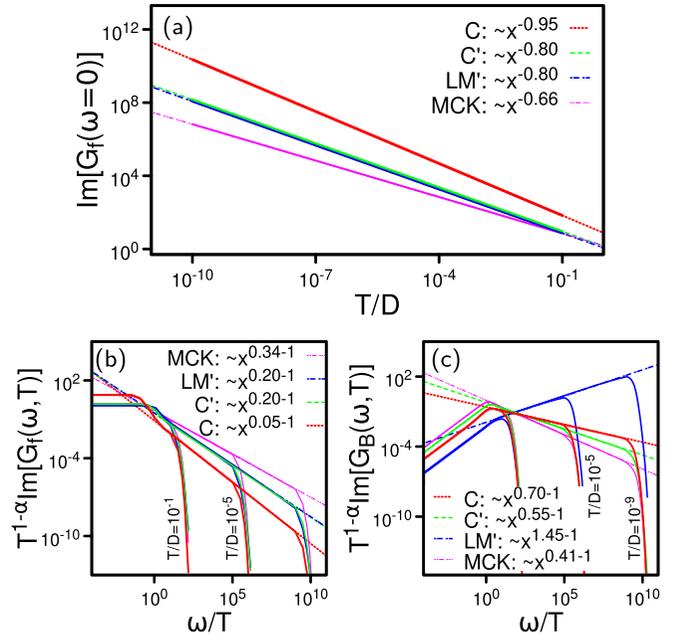

FIG. 4. (a) Temperature dependency of $\mathrm{Im}[G_f(\omega = 0)]$ and the power-law fitting at different fixed points. (b), (c) ω/T-scaling behavior of $G_f(\omega)$ and $G_B(\omega)$ with the exponent obtained from scaling ansatz.
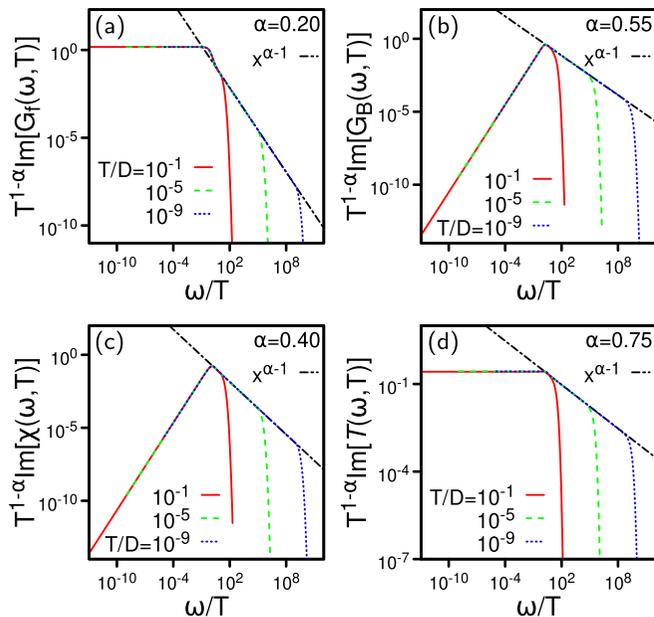
FIG. 5. Numerical results of ω/T-scaling at C′ fixed point for (a) $G_f(\omega)$, (b) $G_B(\omega)$, (c) $\chi(\omega)$, (d) $\mathcal{G}(\omega)$. The parameters are $r = \frac{1}{4}, \epsilon = \frac{2}{5}, \kappa = \frac{1}{2}$.

The imaginary-time (τ) dependence of the various correlation functions is obtained from

$$\Phi(\tau, T) = -\eta \int d\omega \frac{e^{-\omega\tau}}{e^{-\omega/T} - \eta} \text{Im}[\Phi(\omega + i0^+, T)], \quad (40)$$

where $0 < \tau \leqslant 1/T$ and $\eta = -$ ($\eta = +$) for a fermionic (bosonic) correlation function. The τ dependence of $G_f(\tau, T)$ and $G_B(\tau, T)$ at the intermediate fixed points C, C′, LM′, and MCK is shown in Fig. 6. It follows that the Green functions $G_f(\tau, T)$ and $G_B(\tau, T)$ collapse in terms of $\pi T / \sin(\pi\tau T)$ at the intermediate fixed points C, C′, LM′, and MCK. It follows that local multiparticle correlators display a related scaling due to a Wick-type decomposition of higher correlation functions, valid at the saddle point, in terms of $G_f(\tau, T)$ and $G_B(\tau, T)$. The observed scaling to leading order is compatible
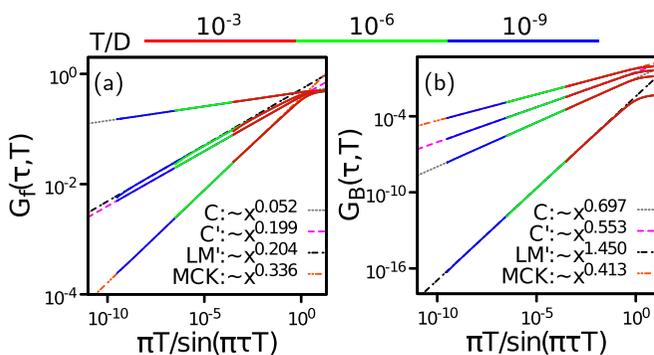

FIG. 6. Numerical results of Green's function with leading power-law fitting at different fixed points. (a) $G_f(\tau, T)$. (b) $G_B(\tau, T)$ at the intermediate fixed points C, C′, LM′, and MCK. The dashed lines indicate the leading power-law behavior. The exponent is in line with α_f and α_B from Table I.

with

$$G_a(\tau) = -\left(\frac{\pi\tau_0 T}{\sin(\pi\tau T)}\right)^\zeta (0 < \tau < 1/T) \quad (41)$$

for $a = f, B$ and with the scaling exponent $0 < \zeta < 1$ such that the results of Appendix. D apply. Such scaling collapse is reminiscent of the one expected for a boundary conformal field theory and would suggest that the boundary entropy in the pseudogap BFKM respects the g-theorem. As will be discussed in the next section, we do, however, observe an extra contribution to Eq. (41) in the dissipative regime, i.e., for $T > \omega$, which is compatible with ω/T-scaling but affects $G_a(\tau, T)$ near $\tau \approx 1/(2T)$. As a result, the g-theorem is violated in the pseudogap BFKM.

B. Boundary entropy

Having established the behavior of G_f and G_B in the vicinity of the intermediate fixed points C, C′, LM′, and MCK, we are in a position to obtain the boundary entropy at the various fixed point and assess the applicability of the g-theorem to the pseudogap BFKM at the large-N level. This theorem addresses the behavior of the impurity entropy along RG trajectories and states that the value of s decreases along the RG flow which has been rigorously proven for boundary conformal models [53,56]. An earlier study of the pseudogap BFKM in the limit of large N concluded that the g-theorem is obeyed [46]. In contrast, our analysis reveals that the g-theorem does not apply to this model.

The results of Ref. [46] are based on Eq. (36) and the conformal scaling form, Eq. (41), which together result in

$$s^* = \int_0^1 \frac{du}{\pi} \frac{2}{u^2 - 1} \left\{ -\frac{\kappa}{u} \arctan\left[u\cot\left(\frac{\pi\alpha_B}{2}\right)\right] \right.$$
$$+ \kappa \arctan\left[\cot\left(\frac{\pi\alpha_B}{2}\right)\right] + u \arctan\left[u\cot\left(\frac{\pi\alpha_f}{2}\right)\right]$$
$$\left. - \arctan\left[\cot\left(\frac{\pi\alpha_f}{2}\right)\right] \right\} \quad (42)$$

for the $T = 0$ boundary entropy at a fixed point with exponents α_f and α_B for G_f and G_B, respectively.

Before turning to our results for the fixed-point entropy at the various intermediate fixed points, we will discuss several benchmarks to demonstrate the reliability of our evaluation which is based on Eq. (25).

The degeneracy of the weak coupling fixed point LM at $J_K = 0 = g$, $N!/(Q!(N-Q)!)$ is tied to the constraint associated with the totally antisymmetric representation $\sum_{\sigma=1}^N f_\sigma^\dagger f_\sigma = Q$. The associated boundary entropy is thus $s_{LM} = \ln 2$ as we have chosen $Q = N/2$. For the special case $r = 0$, $g = 0$, as discussed by Parcollet et al., the strong coupling fixed point of the model is amenable to a conformal field theory description, which, for $Q = N/2$, results in $s_{MCK}^{r=0} = (1 + \kappa)[f(1 + \kappa) - 2f(2 + 2\kappa)]/\pi$, where

$$f(x) = \int_0^{\pi/x} du \ln(\sin u) \quad (43)$$

(see Ref. [50] for details).

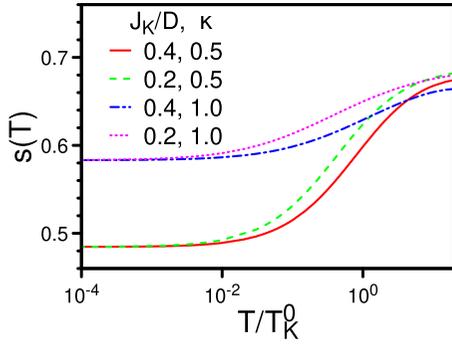Figure 7 shows that our evaluation of $s(T)$ in the special case with ($r = 0$, $g = 0$) of the (pseudogap) BFKM indeed

FIG. 7. The impurity entropy $s(T)$ for $r = 0$ and $g = 0$ vs T/T_K^0 for $r = 0$. The fixed-point values at MCK [$s(T = 0)$] and LM [$s(T/T_K^0 \to \infty)$] are recovered independently of the value of J_K. $s(T = 0)$ depends on $\kappa = M/N$ (see Ref. [50]).

reproduces s_{LM} and $s_{\mathrm{MCK}}^{r=0}$ for given κ, independently of J_K. A further test is provided by evaluating the entropy in the large-N version of the Sachdev-Ye-Kitaev (SYK) model, which is defined by $\Sigma(\tau) = -J^2 G(-\tau)^3$, together with the Dyson equation, linking G and Σ and where J is a coupling constant. As discussed in detail in Appendix F, our calculation of the entropy $s_{\mathrm{SYK}}(T)$ in the SYK model reproduces the analytical prediction for $T = 0$ and high T [67]. Appendix F also contains a discussion of the scaling properties of G and Σ.

Having established the reliability of Eq. (25) in evaluating the boundary entropy, we can apply it to the generic peudogap BFKM with $r \neq 0$, $\epsilon \neq 0$ and arbitrary J_K and g. In Fig. 8, we show typical results for $r = \frac{1}{4}$, $\epsilon = \frac{2}{5}$, $\kappa = \frac{1}{2}$ and a range of coupling constants that lead to flows to different fixed points. One can infer from the results shown in Fig. 8 that fixed-point LM' is characterized by an impurity entropy that is considerably larger than that associated with the other fixed points. A comparison of the values of $s(T = 0)$ with Fig. 1 implies that the RG flow toward LM' is in contradiction to expectations based on g-theorem. The same is true for, e.g., the RG flow from C to C'. Thus, we conclude that the g-theorem is not fulfilled in the pseudogap BFKM. As both the pseudogap DOS and the power spectral density of the bosonic bath (with short-ranged coupling constants J_K and g) break conformal
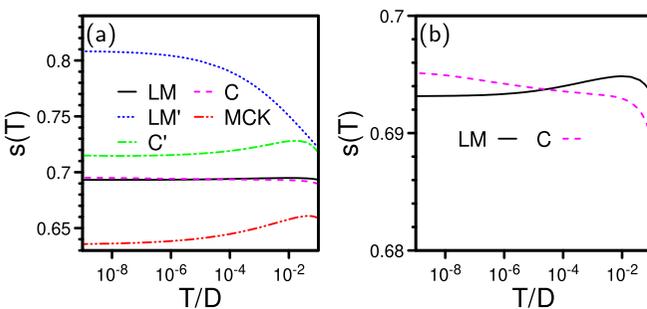

FIG. 8. (a) Boundary entropy of the pseudogap BFKM model for $r = \frac{1}{4}$, $\epsilon = \frac{2}{5}$, $\kappa = \frac{1}{2}$ and coupling constants J_K and g such that $s(T = 0) = s_{\mathrm{MCK}}$ for $J_K = 0.7D$, $g = 0$, $s(T = 0) = s_{\mathrm{LM}}$ for $J_K = 0.325D$, $g = 0$, $s(T = 0) = s_C$ for $J_K = 0.45D$, $g = 0$, $s(T = 0) = s_{C'}$ for $J_K = 0.8D$, $g = 0.375D$, and $s(T = 0) = s_{\mathrm{LM'}}$ for $J_K = 0$, $g = 0.325D$. (b) Same as (a) for values of $s(T \to 0)$ between 0.68 and 0.7 to show the differences between s_C and s_{LM}.
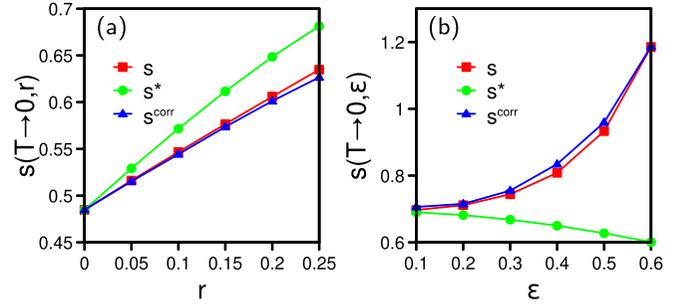

FIG. 9. Comparison of different approach of determining the residual boundary entropy, labeled by s, s^*, and s^{corr}. The specifics of each of these approaches are given in the main text. (a) r dependence of s, s^*, and s^{corr} at the MCK fixed point and (b) ϵ dependence of s, s^*, and s^{corr} at the LM' fixed point with difference ϵ.

invariance of the Hamiltonian, this conclusion may not be completely unexpected.

C. Scaling function and entropy flow

Can we understand why Eq. (42) is inappropriate to evaluate the residual boundary entropy of the pseudogap BFKM? In Fig. 9, we show s^*, obtained from evaluating Eq. (42) together with $s(T \to 0)$ based on expression Eq. (25), and s^{corr} which is obtained from a correction scheme to be outlined below. In Fig. 9(a), this comparison is shown as a function of r for the pseudogap MCK fixed point while Fig. 9(b) contrast $s(T \to 0)$ and s^{corr} with s^* as a function of ϵ. Clearly, the difference between s^* and $s(T \to 0)$ grows with r for MCK and with ϵ for LM'.

In order to trace the origin of this difference, we compare $a_f(\omega/T) = \arctan \frac{G_f'(\omega,T)}{G_f''(\omega,T)}$, evaluated with the self-consistently determined G_f and with the analytically continued Fourier transform of Eq. (41), determined in Appendix D, for the pseudogap MCK and the LM' fixed points. It is worth noting that this comparison is parameter free. As shown in Fig. 10 there is by and large good agreement for G_f near the pseudogap MCK fixed point for $r = 0.2$, shown in Fig. 10(a) and near LM' for $\epsilon = 0.5$, depicted in Fig. 10(b). This overall good agreement is also implied by the results shown in Fig. 6. The deviations occurring for large argument, i.e., for $\omega \gg T$, are caused by the high-energy cutoff of the scaling regime and are also visible in Fig. 4. Outside of the scaling regime, a_f no longer shows ω/T-scaling. A further difference becomes visible when zooming into the quantum dissipative regime where $\omega < T$, as shown in Fig. 10(c) for MCK and Fig. 10(d) for LM'. This deviation grows with r [see Fig. 10(c)] and with ϵ as demonstrated in Fig. 10(d). Our conclusion that this difference underlies the discrepancy between $s(T \to 0)$ and s^* is further corroborated by using the numerical $a_f(\omega/T)$ and $a_B(\omega/T)$ in Eq. (36) and ignoring the part outside of the scaling regime for $\omega \gg T$. This leads to an estimate for the residual boundary entropy which is called s^{corr} in Fig. 9 and which agrees well with $s(T \to 0)$.

The correction to Eq. (41) shown in Fig. 10(c) for MCK and Fig. 10(d) for LM' is confined to the quantum dissipative regime where $T \gg \omega$. This suggests that this correction
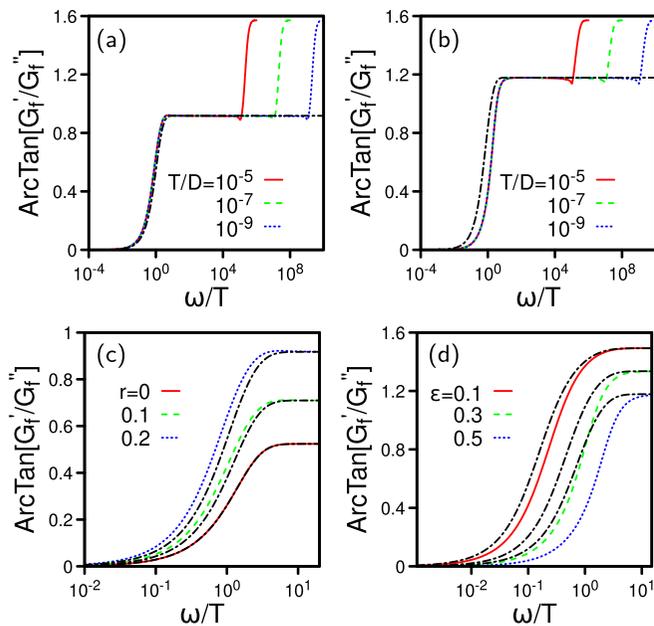
FIG. 10. Comparison of arctan [Re{G_f}/Im{G_f}] obtained from Eq. (41) and denoted by black dashed-dotted lines with results obtained from self-consistent solutions of the saddle-point equations. (a) Comparison for $r = 0.2$ at the MCK fixed point. (b) Comparison for $\epsilon = 0.5$ at the LM′ fixed point. (c) r-dependent comparison at the MCK fixed point at low T and for $\omega \lesssim T$. (d) ϵ-dependent comparison at the LM′ fixed point at low T and for $\omega \lesssim T$.

vanishes as $T \to 0$. At $T \neq 0$, it does, however, lead to a linear-in-T contribution to the free energy and thus a contribution to the residual boundary entropy s. For this reason, we will refer to the contribution for $\omega < T$ shown in Fig. 10 as anomalous. The results from the scaling ansatz which, strictly speaking, operates at $T = 0$ but its results apply to the quantum coherent regime, i.e., where $\omega \gg T$ are in line with this conclusion. As discussed in Appendix E, where the scaling ansatz is extended to the next leading order, no anomalous term appears in the $T = 0$, $\omega \to 0$ solution of the self-consistency equations.

In order to understand the effect of the anomalous contribution on $G(\tau)$, it is useful to notice that the kernel of Eq. (40) for $\tau = 1/(2T)$ is equal to $\{2 \cosh [\omega/(2T)]\}^{-1}$.

Thus, $G(\tau = 1/(2T))$ is primarily determined by $G(\omega, T)$ in the hydrodynamic regime. For a function G that displays ω/T-scaling, i.e., $G(\omega, T) = T^{\alpha-1}\Phi(\omega/T)$, it follows from Eq. (40) that $G(\tau, T) = T^\alpha \widetilde{\Phi}(\tau T)$. In Fig. 11, we plot $\widetilde{\Phi}(\tau T)$ as a function of $[\pi/\sin(\pi\tau T)]^\alpha$. Figure 11(a) shows that in terms of $x = [\pi/\sin(\pi\tau T)]^\alpha$,

$$\widetilde{\Phi}(x) \sim x \qquad (44)$$

in the scaling regime except for the region near $x \approx \pi^\alpha$ which corresponds to $\tau \approx 1/(2T)$, where a tiny deviation from $\widetilde{\Phi}(x) \sim x$ occurs as shown in Fig. 11(b). For comparison, we provide a plot similar to Fig. 11 for MCK in the conformally invariant $r = 0$ case (see Fig. 14). It is the deviation from $\widetilde{\Phi}(x) \sim x$ that corresponds to the anomalous contribution shown in Fig. 10(b). For $\tau \to 0^+$, corresponding to large x, $G_f(\tau)$ is fixed by the constraint so that the T dependence
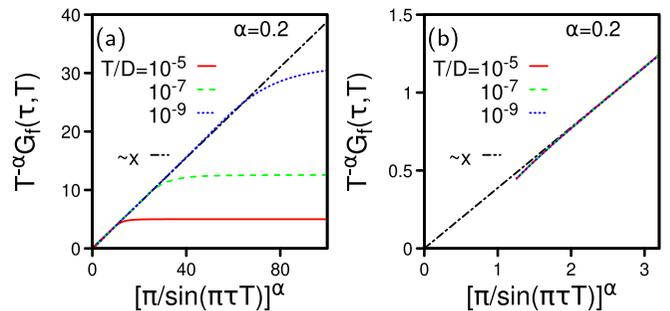

FIG. 11. The behavior of $G_f(\tau)$ of LM′ fixed point with $\epsilon = 0.4$. (a) The temperature dependency and (b) near $\beta/2$ regime.

in Fig. 11(a) for large values of x has to be $\sim T^\alpha$. The part in Fig. 11, on the other hand, that obeys $\widetilde{\Phi}(x) \sim x$, is compatible with the scaling of Eq. (41).

D. $T \neq 0$ behavior of the boundary entropy

Having analyzed the fate of the g-theorem in the pseudogap BFKM and traced back the origin of the inapplicability of the g-theorem to the scaling function, we turn to the ramifications for the $T \neq 0$ behavior of the boundary entropy.

Generically, one expects an entropy accumulation near a QCP, i.e., tuning the system across the critical coupling $g = g_c$ on an isentropic $T_{s=\text{const}}(g)$ at low but nonvanishing T one expects a minimum close to g_c. If the g-theorem is fulfilled, one expects that $s(T)$ decreases as T is lowered while models that defy it show an increase in $s(T)$ as T decreases [56,68].

In Fig. 12, the boundary entropy $s(T)$ is shown at nonzero T across the phase diagram of the pseudogap BFKM. As shown in Fig. 12(a), where $s(T = 10^{-7}D)$ is shown as a function of the coupling constants J_K and g, LM′ gives rise to a phase with an enhanced s compared to the value of s near MCK and the separatrix between MCK and LM′, where it is controlled by the flow to C′. Consequently, due to the inapplicability of the g-theorem for $g \neq 0$, one does not observe an entropy accumulation above C′. Instead, as the system flows from the vicinity of C′ at an elevated T to LM′ as $T \to 0$, the boundary entropy (T) increases. In contrast, for $g = 0$, the pseudogap BFKM fulfills the g-theorem and this is reflected in the finite-T values of s vs J_K, which is demonstrated in Fig. 12(c). For completeness, Figs. 12(d) and 12(e) show the boundary entropy $s(T)$ vs T and J_K near MCK [in Fig. 12(d)] and T and g near LM′ [in Fig. 12(e)].

VI. SUMMARY

We have studied the impurity entropy of the spin-isotropic pseudogap Bose-Fermi Kondo model in a dynamical large-N limit. Our primary focus in this study has been the applicability of the g-theorem which relates the residual boundary entropy to the RG flow to the pseudogap Bose-Fermi Kondo model. For the g-theorem to be valid, the boundary entropy has to decrease along RG trajectories. The pseudogap Bose-Fermi Kondo Hamiltonian lacks conformal invariance due to the pseudogap density of states of the fermionic bath as well as the sub-Ohmic spectral density of the bosonic bath
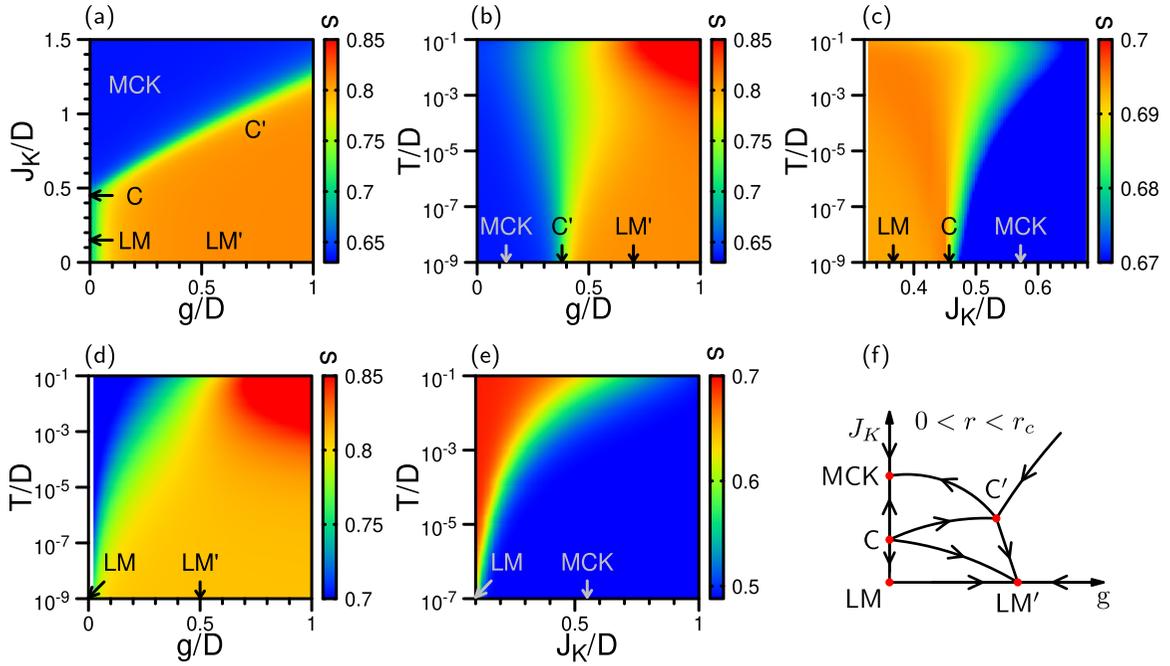
FIG. 12. (a) Boundary entropy $s(J_K, g, T_0)$ at $T_0 = 10^{-7}D$ as a function of J_k and g. (b) $s(J_K^0, g, T)$ across C′ at $J_k^0 = 0.8D$ vs g and T. (c) $s(J_K, g = 0, T)$ across C vs J_k and T. (d) $s(J_K = 0, g, T)$ near LM′ vs g and T. (e) $s(J_K, g = 0, T)$ near the MCK of $r = 0$ case vs J_k and T. (f) Flow diagram for $0 < r < r_c$ case.

which would otherwise guarantee that the model fulfills the g-theorem.

We addressed the problem by evaluating the impurity entropy at the large-N level directly from the free energy in that limit and showed that this method is equivalent to a Luttinger-Ward-based approach. The correctness of our entropy evaluation is substantiated by applying it to the large-N limits of the standard $SU(N) \times SU(M)$ symmetric Kondo model and the Sachdev-Ye-Kitaev model where exact results for the impurity entropy are available.

In the pseudogap Bose-Fermi Kondo model, energy-over-temperature (ω/T) scaling is found at all intermediate fixed points. We also found a scaling form in τT for local, i.e.,

impurity correlators which implies ω/T-scaling and appears to be compatible with that obtained from boundary conformal field theory and which is, e.g., shown in Fig. 6.

On top of scaling form in τ/β we also identified an anomalous contribution in the regime where $\hbar\omega < k_B T$, i.e., in the so-called hydrodynamic regime and which is absent in the quantum coherent regime ($\hbar\omega > k_B T$), where the asymptotically exact scaling behavior is amenable to the scaling ansatz summarized in Appendix E. This contribution is present at all nontrivial fixed points except for the multichannel Kondo fixed point for $r = 0$ but is largest for LM′.

Our main conclusion is the finding that the g-theorem is not obeyed in the pseudogap Bose-Fermi Kondo model at the large-N level. We traced this violation back to the anomalous contribution to the large-N scaling functions. As a result, entropy accumulation is generally not observed at the critical
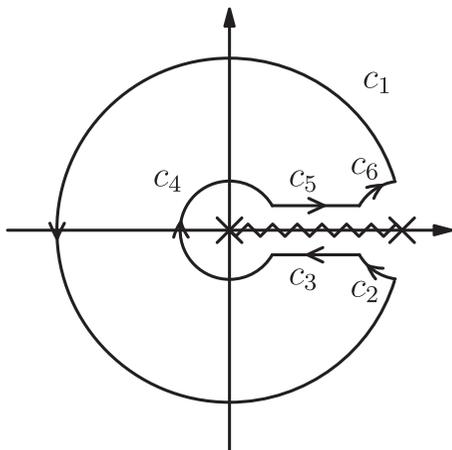

FIG. 13. The contour $\mathcal{C} = c_1 + c_2 + c_3 + c_4 + c_5 + c_6$ used to evaluate the integral (D4).
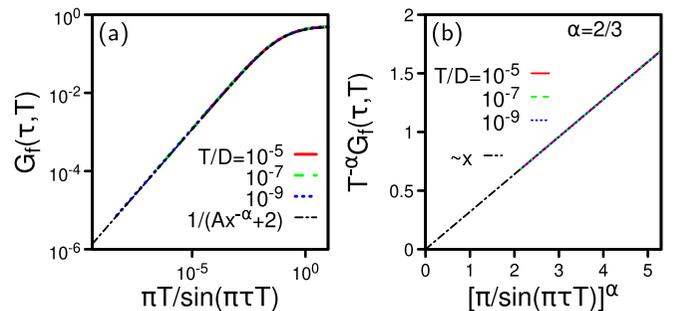

FIG. 14. Behavior of $G_f(\tau)$ for the $r = 0$ MCK fixed point case. (a) $G_f(\tau)$ at various temperatures. The black dashed line is the fitting of $G_f(\tau)$ with $\frac{1}{Ax^{-\alpha_f}+2}$ at $r = 0$ case. (b) Behavior of $G_f(\tau)$ near $\beta/2$ regime.

fixed point located at intermediate couplings (C′ in our notation and located at J_K^*, g^*) as the residual boundary entropy at LM′ is larger than that at C′ (see, e.g., Fig. 8). Instead, we are able to observe an impurity entropy decrease as temperature rises for certain parameter ranges of the model.

The results reported here are based on the large-N method and anchored around $N \rightarrow \infty$. How our results generalize to finite values of N is not only a relevant but also a largely open question. Where a comparison is possible, the direct comparison of the leading behavior between the SU(N)-symmetric large-N limit utilized here and the SU(2) case indicates that the large-N limit is regular and yields results that are close to those of the SU(2) case, at least for $r = 0$ [38]. On the other hand, no anomalous correction to the scaling function of Eq. (41) of the type we discussed here appears in essentially exact Monte Carlo studies of the finite-N counterparts [24,25,38,48].

One possibility to reconcile these two observations could be that the singular behavior is subleading. After all, the issue of singularities within the large-N approach is delicate and cases are known where the leading-order behavior in N appears to be regular while subleading corrections turn out to be singular [69]. This possibility is also in line with the following observation: The critical point C′ for $r = 0$ and $\epsilon \rightarrow 1^-$ describes the critical Kondo destruction observed in a class of heavy electron materials within the extended dynamical mean field approach [5,9,10]. The residual entropy s in the easy-axis and SU(2)-symmetric cases of the $r = 0$ Bose-Fermi Kondo model is known to vanish in the limit $\epsilon \rightarrow 1^-$ [70]. In contrast, at the large-N level, longitudinal fluctuations are subleading and s remains finite as $\epsilon \rightarrow 1^-$.

An interpretation of the g-theorem in a quantum information theory context has recently been provided [71]. In light of this interpretation, the results of Ref. [72] appear to be consistent with the conclusion that the g-theorem is not fulfilled even in models of critical Kondo destruction away from the large-N limit investigated here.

APPENDIX A: DYNAMICAL LARGE N

The overall strategy of the dynamical large-N approach is to cast the action into a form $S = NS_{\text{eff}}$ so that the saddle-point approximation becomes exact in the limit $N \rightarrow \infty$. We start from the action of the SU(N) × SU(M)-symmetric pseudogap

BFKM [Eq. (8)]

$$
\begin{aligned}
S^{\text{DLN}} = & -\int_\tau c_{k\alpha\sigma}^\dagger g_c^{-1} c_{k'\alpha\sigma} + \Phi_q^\dagger g_\Phi^{-1} \Phi_q + f_\sigma^\dagger g_f^{-1} f_\sigma \\
& + \int_\tau \frac{J_K}{N} f_\sigma^\dagger f_{\sigma'} c_{k\sigma'\alpha}^\dagger c_{k'\sigma\alpha} - \lambda q_0 N \\
& + \frac{g}{\sqrt{N}} f_\sigma^\dagger f_{\sigma'} \tau_{\sigma\sigma'}^i \big(\Phi_q^{i\dagger} + \Phi_q^i\big).
\end{aligned} \tag{A1}
$$

Introducing a bosonic Hubbard-Stratonovich field B to decouple the Kondo interaction and integrating out the c and Φ fields leads to

$$
\begin{aligned}
S^{\text{DLN}} = & \int_{\tau,\tau'} \sum_\sigma f_\sigma^\dagger(\tau)(-g_f^{-1}(\tau,\tau')) f_\sigma(\tau') \\
& + \int_{\tau,\tau'} \sum_\alpha B_\alpha^\dagger(\tau) \frac{1}{J_K} \delta(\tau-\tau') B_\alpha(\tau') \\
& + \int_{\tau,\tau'} \sum_{\alpha\sigma} \left[B_\alpha(\tau) f_\sigma^\dagger(\tau) \sum_{kk'} \frac{g_c(\tau,\tau')}{N} f_\sigma(\tau') B_\alpha^\dagger(\tau') \right] \\
& + \int_{\tau,\tau'} \frac{g^2}{N} \sum_{q\sigma\sigma'} f_\sigma^\dagger(\tau) f_\sigma(\tau')(-g_\Phi(\tau,\tau')) f_{\sigma'}^\dagger(\tau') f_{\sigma'}(\tau) \\
& + (N^2-1)\text{Tr}\ln\big(-g_\Phi^{-1}\big) - M\,\text{Tr}\ln\frac{1}{J_K} - q_0 N \int_\tau \lambda(\tau) \\
& - g^2 q_0^2 \sum_q \int_{\tau,\tau'} g_\Phi(\tau,\tau') - NM\,\text{Tr}\ln\big(-g_c^{-1}\big).
\end{aligned} \tag{A2}
$$

Additional Hubbard-Stratonovich fields Q and W are introduced to decouple the two quartic terms in the previous expression. Thus,

$$
\begin{aligned}
S^{\text{DLN}} = & \int_{\tau,\tau'} N\bar{Q}(\tau,\tau') Q(\tau',\tau) + \int_{\tau,\tau'} N\bar{W}(\tau',\tau) W(\tau,\tau') \\
& + \int_{\tau,\tau'} \sum_\alpha B_\alpha^\dagger(\tau)\big(-G_B^{-1}(\tau,\tau')\big) B_\alpha(\tau') \\
& + \int_{\tau,\tau'} \sum_\sigma f_\sigma^\dagger(\tau)\big(-G_f^{-1}(\tau,\tau')\big) f_\sigma(\tau') - q_0 N \int_\tau \lambda(\tau) \\
& + (N^2-1)\text{Tr}\ln\big(-g_\Phi^{-1}\big) - M\,\text{Tr}\ln\frac{1}{J_K} \\
& - g^2 q_0^2 \sum_q \int_{\tau,\tau'} g_\Phi(\tau',\tau) - NM\,\text{Tr}\ln\big(-g_c^{-1}\big),
\end{aligned} \tag{A3}
$$

where G_f^{-1} and G_B^{-1} are defined as

$$
\begin{aligned}
G_f^{-1}(\tau,\tau') = & g_f^{-1}(\tau,\tau') - \bar{Q}(\tau,\tau') - g g_\Phi(\tau,\tau') W(\tau,\tau') \\
& - g\bar{W}(\tau,\tau'), \\
G_B^{-1}(\tau,\tau') = & -\frac{1}{J_K}\delta(\tau-\tau') + g_c(\tau',\tau) Q(\tau,\tau').
\end{aligned} \tag{A4}
$$

Integrating out B and f fields leads to

$$
S^{\mathrm{DLN}} = \int_{\tau,\tau'} N\bar{Q}(\tau,\tau')Q(\tau',\tau) + \int_{\tau,\tau'} N\bar{W}(\tau',\tau)W(\tau,\tau')
$$

$$
+ M\,\mathrm{Tr}\,\ln\left(-G_B^{-1}\right) - N\,\mathrm{Tr}\,\ln\left(-G_f^{-1}\right) - M\,\mathrm{Tr}\,\ln\frac{1}{J_K}
$$

$$
+ (N^2-1)\mathrm{Tr}\,\ln\left(-g_\Phi^{-1}\right) - q_0 N\int_\tau \lambda(\tau)
$$

$$
- g^2 q_0^2 \sum_q \int_{\tau,\tau'} g_\Phi(\tau',\tau) - NM\,\mathrm{Tr}\,\ln\left(-g_c^{-1}\right)
$$

$$
= NS_{\mathrm{eff}}. \tag{A5}
$$

Upon discarding terms independent of B, f, and λ, one is led to

$$
S_{\mathrm{eff}} = \int_{\tau,\tau'} \bar{Q}(\tau,\tau')Q(\tau',\tau) + \bar{W}(\tau',\tau)W(\tau,\tau')
$$

$$
+ \frac{M}{N}\mathrm{Tr}\,\ln\left(-G_B^{-1}(\tau,\tau')\right)
$$

$$
- \mathrm{Tr}\,\ln\left(-G_f^{-1}(\tau,\tau')\right) - q_0\int_\tau \lambda(\tau). \tag{A6}
$$

This form of the action is suitable for taking the saddle-point limit $\delta_{Q,\bar{Q},W,\bar{W},\lambda} S_{\mathrm{eff}} = 0$ which results in a set of equations

$$
\begin{aligned}
Q(\tau) &= -G_f(\tau), \\
\bar{Q}(\tau) &= -\kappa G_B(\tau)g_c(\tau), \\
W(\tau) &= -gG_f(\tau), \\
\bar{W}(\tau) &= -gG_f(\tau)g_\Phi(-\tau),
\end{aligned} \tag{A7}
$$

which become exact in the limit $N \to \infty$. This set of equations is augmented by the constraint $G_f(\tau \to 0^-) = q$ that results from the fully antisymmetric representation of the impurity spin algebra. Note that at the saddle-point level, λ is independent of τ.

APPENDIX B: DETAILS OF THE BOUNDARY ENTROPY CALCULATION

In this Appendix, we detail the derivation of Eq. (24) for the boundary entropy. From the definition of the impurity entropy s, we have

$$
s = -\frac{df_{\mathrm{imp}}}{dT} = -\frac{\partial f_{\mathrm{imp}}}{\partial T} - \sum_{X_i} \frac{\delta f_{\mathrm{imp}}}{\delta X_i}\frac{\partial X_i}{\partial T}, \tag{B1}
$$

where X_i runs over the set $\{\bar{Q}, Q, \bar{W}, W, \lambda\}$. The saddle-point conditions imply that the sum over X_i vanishes. Thus, we can obtain s without considering the T dependence of the set $\{\bar{Q}, Q, \bar{W}, W, \lambda\}$. Starting from

$$
f_{\mathrm{imp}} = \int_\tau \bar{Q}(\tau)Q(-\tau) + \bar{W}(-\tau)W(\tau) - q_0\lambda(\tau)
$$

$$
+ T\kappa\,\mathrm{Tr}\,\ln\left(-G_B^{-1}\right) - T\,\mathrm{Tr}\,\ln\left(-G_f^{-1}\right), \tag{B2}
$$

and transforming to real frequencies, one can take perform the derivative with respect to T on the distribution functions once G_B and G_f have been expressed in terms of $\{\bar{Q}, Q, \bar{W}, W, \lambda\}$. As a result,

$$
s^{\mathrm{DLN}} = -\int \frac{d\omega}{\pi}\partial_T\left\{n_b(\omega)\kappa\,\mathrm{Im}\left[\ln\left(-G_B^{-1}(\omega)\right)\right] + n_f(\omega)\mathrm{Im}\left[\ln\left(-G_f^{-1}(\omega)\right)\right] + n_f(\omega)\mathrm{Im}[\bar{Q}(\omega)Q(\omega)] - n_f(\omega)\mathrm{Im}[\bar{W}(\omega)W(\omega)]\right\}
$$

$$
= -\int \frac{d\omega}{\pi}\left\{\frac{dn_b(\omega)}{dT}\kappa\,\mathrm{Im}\left[\ln\left(-G_B^{-1}(\omega)\right)\right] + n_b(\omega)\kappa\,\mathrm{Im}[-G_B(\omega)\partial_T(Q(\tau)g_c(-\tau))_\omega]\right.
$$

$$
+ \frac{dn_f(\omega)}{dT}\mathrm{Im}\left[\ln\left(-G_f^{-1}(\omega)\right)\right] + n_f(\omega)\mathrm{Im}[-G_f(\omega)\partial_T(gW(\tau)g_\Phi(\tau))_\omega]
$$

$$
\left.+ \frac{dn_f(\omega)}{dT}\mathrm{Im}[\bar{Q}(\omega)Q(\omega)] - \frac{dn_f(\omega)}{dT}\mathrm{Im}[\bar{W}(\omega)W(\omega)]\right\}. \tag{B3}
$$

The saddle-point condition implies $Q(\tau) = G_f(\tau)$, $W(\tau) = -gG_f(\tau)$, $\bar{Q}(\tau) = \Sigma_f^1(\tau)$, and $\bar{W}(\tau) = \Sigma_f^2(\tau)/2$, in terms of which Eq. (B3) reduces to Eq. (24).

APPENDIX C: EQUIVALENCE OF THE DYNAMIC LARGE-*N* LIMIT WITH AN ASSOCIATED CONSERVING KADANOFF-BAYM SCHEME

In this Appendix we explicitly demonstrate the equivalence of the dynamical large-*N* approach with that based on a conserving approximation regarding the calculation of the impurity entropy. Conserving approximations are invariant with respect to a set of symmetry transformations and respect the related Ward identities which link vertex corrections

and self-energies at each order of perturbation theory. Within the Kadanoff-Baym approach, conserving approximations are constructed through the stationary condition of an associated Luttinger-Ward functional Φ. Φ derivability of an approximation is often taken to be tantamount to it being conserving [61]. It was pointed out in Ref. [73] that a principal difference exists between the Kadanoff-Baym and a true large-*N* scheme. It was already shown in Eq. (21) that the saddle-point free energy at the dynamical large-*N* level naturally assumes the form of the Legendre transform of a Luttinger-Ward functional. Given the importance of a faithful determination of the residual boundary entropy for assessing the validity of the *g*-theorem, we derive explicitly Eq. (24) from the large-*N* equations.

At leading order in N, the Luttinger-Ward functional $\Phi(G)$ is given by

$$\Phi(G) = -\int d\tau \{ \boldsymbol{v}^\dagger [\boldsymbol{G}_B(\tau) \otimes \boldsymbol{G}_f(-\tau) \otimes \boldsymbol{g}_c(\tau)] \boldsymbol{v}$$
$$+ \boldsymbol{w}^\dagger [\boldsymbol{G}_f(\tau) \otimes \boldsymbol{G}_f(-\tau) \otimes \boldsymbol{g}_\Phi(\tau)] \boldsymbol{w} \} \quad (C1)$$

with $v^{\alpha_B, \alpha_c}_{\sigma_f, \sigma_c} = 1/\sqrt{N} \delta_{\sigma_f, \sigma_c} \delta_{\alpha_B, \alpha_c}$ and $w^i_{\sigma_f, s_f} = g t^i_{\sigma_f, s_f}/\sqrt{N}$ together with the constraint $\boldsymbol{G}_f(\tau \to 0-) = q\boldsymbol{1}$ [the set $\{t^i\}$ $(1, \ldots N^2 - 1)$ was defined in Eq.(5)] [see also Eq. (21)]. The constitutive relation $\delta\Phi(G) = -T \text{Tr}[\Sigma \delta G]$ together with the assumption that $\boldsymbol{G}_B$, $\boldsymbol{G}_f$, $\boldsymbol{g}_c$, and $\boldsymbol{g}_\Phi$ are diagonal in their respective indices, results in Eqs. (16) and (17). The impurity contribution to the free energy is given by

$$f_{\text{imp}}^{\text{KB}} = T \left\{ \text{Tr}\left[\kappa \ln\left(-G_B^{-1} \right) - \ln\left(-G_f^{-1} \right) \right] \right\} - \lambda q_0$$
$$+ \int d\tau \{ \kappa \left[g_B^{-1}(-\tau) - G_B^{-1}(-\tau) \right] G_B(\tau)$$
$$- \left[g_f^{-1}(\tau) - G_f^{-1}(\tau) \right] G_f(-\tau) \} + \Phi(G) \quad (C2)$$

computed at the extremal points where $\delta f_{\text{imp}}/\delta G_a = 0$ and $\partial f_{\text{imp}}/\partial\lambda = 0$. When taking the derivative of f_{imp} with respect to T, we can ignore the dependence of G_f, G_B, and λ on T by virtue of these stationary conditions (see Appendix B). The impurity entropy is thus given by [62,63]

$$s^{\text{KB}} = -\int \frac{d\omega}{\pi} \frac{dn_b}{dT} \{ \kappa \left[\text{Im} \ln\left(-G_B^{-1} \right) + \text{Im}\Sigma_B \text{Re} G_B \right]$$
$$- \text{Re}\tilde{\Sigma}_\Phi \text{Im} g_\Phi \} + \frac{dn_f}{dT} \left[\text{Im} \ln\left(-G_f^{-1} \right) + \text{Im}\Sigma_f \text{Re} G_f \right]$$
$$- \kappa \, \text{Re}\tilde{\Sigma}_c \text{Im} g_c \right], \quad (C3)$$

where the auxiliary quantities $\tilde{\Sigma}_c(\tau) = N\Sigma_c(\tau) = -G_B(-\tau)G_f(\tau)$ and $\tilde{\Sigma}_\Phi(\tau) = \frac{1}{N}\Sigma_\Phi(\tau) = g^2 G_f(\tau)G_f(-\tau)$ are used. By construction, the constitutive relation reproduces the dynamical large-N equations of Eq. (A7). From the identity

$$n_b(\nu)[n_f(\omega) - n_f(\omega - \nu)] = -n_f(\omega)n_f(-\omega + \nu) \quad (C4)$$

it follows that

$$n_b(\nu)\frac{d}{dT}[n_f(\omega) - n_f(\omega - \nu)]$$
$$= -\frac{dn_f(\omega)}{T}n_f(-\omega + \nu) - n_f(\omega)\frac{dn_f(-\omega + \nu)}{dT}$$
$$- \frac{dn_b(\nu)}{dT}[n_f(\omega) - n_f(\omega - \nu)], \quad (C5)$$

by taking the derivative with respect to T. This further implies

$$\int \frac{d\nu}{\pi} n_b(\nu)\kappa \, \text{Im}[G_B(\nu)\partial_T A(\omega)]$$
$$= \int \frac{d\nu}{\pi} \left\{ \frac{dn_f(\nu)}{dT}\left[\kappa g_c''(\nu)\tilde{\Sigma}_c'(\nu) + G_f''(\nu)\Sigma_f^{1'}(\nu) \right] \right.$$
$$\left. - \kappa \frac{dn_b(\nu)}{dT}G_B'(\nu)\Sigma_B''(\nu) \right\} \quad (C6)$$

and

$$-\int \frac{d\nu}{\pi} n_f(\nu)\text{Im}[G_f(\nu)\partial_T B(\omega)]$$
$$= \int \frac{d\nu}{\pi} \frac{dn_b(\nu)}{dT}g_\Phi''(\nu)\tilde{\Sigma}_\Phi'(\nu)$$
$$- \int \frac{d\nu}{\pi} \frac{dn_f(\nu)}{dT}g\bar{W}''(\nu)G_f'(\nu)$$
$$+ \int \frac{d\nu}{\pi} \frac{dn_f(\nu)}{dT}g\bar{W}'(\nu)G_f''(\nu). \quad (C7)$$

These last two equations can be used to establish the equivalence of Eq. (C3) with Eq. (24).

APPENDIX D: FOURIER TRANSFORMATION OF $\left(\frac{\pi\tau_0}{\beta \sin(\pi\tau/\beta)}\right)^\zeta$

This Appendix provides details of performing the Fourier transform of

$$\mathcal{G}_a(\tau) = -\left(\frac{\pi\tau_0}{\beta \sin(\pi\tau/\beta)}\right)^\zeta \quad (0 < \tau < \beta) \quad (D1)$$

which is required in the discussion of the entropy results and the scaling ansatz solution. In Eq. (D1), τ_0 acts as a short-time cutoff and has units of inverse energy. The parameter a distinguishes between bosonic ($a = b$) and fermionic functions ($a = f$), i.e.,

$$\mathcal{G}_a(\tau) = -\eta\mathcal{G}_a(\tau + \beta) \quad (D2)$$

for $-\beta < \tau < 0$ with $\eta = -1$ for $a = b$ and $\eta = 1$ for $a = f$. We consider $0 < \zeta < 1$. For fixed τ it follows that in the zero-temperature limit ($\beta \to \infty$) $\mathcal{G}_a(\tau) = -(\tau_0/\tau)^{-\zeta}$. The definition of the Fourier transform of Eq. (D1) is

$$G_a(i\omega_n^a) = \int_0^\beta d\tau \, e^{i\omega_n^a \tau} \mathcal{G}_a(\tau), \quad (D3)$$

with the Matsubara frequencies $\omega_n^b = 2n\pi/\beta$ and $\omega_n^f = (2n + 1)\pi/\beta$ for $n = 0, \pm 1, \pm 2, \ldots$. Equation (D1) can be cast into the form

$$G_a(i\omega_n^a) = -\left(\frac{2\pi i\tau_0}{\beta}\right)^\zeta \int_0^\beta d\tau \, e^{i\omega_n^a \tau + i\pi\zeta\tau/\beta}[e^{2\pi i\tau/\beta} - 1]^{-\zeta}.$$

Performing the substitution $s = e^{2\pi i\tau/\beta}$ maps the integral onto the contour labeled c_1 in Fig. 13. The integrand is singular at $s = 0$ and 1 and we choose to put the connecting branch cut on the real s axis. Thus,

$$I \equiv -\left(\frac{2\pi i}{\beta}\right)^{\zeta-1}\tau_0^\zeta \oint_{\mathcal{C}} dz \, z^{\frac{m_a+\zeta}{2}-1}(z-1)^{-\zeta} = 0, \quad (D4)$$

where $m_a = \beta\omega_n^a/\pi$ and the contour $\mathcal{C} = c_1 + \cdots + c_6$ is depicted in Fig. 13. As long as $\zeta < 1$, the contribution along c_2 and c_6 vanishes as the radii of these two arcs goes to zero. Similarly, as the radius of the circle c_4 shrinks to zero, the contribution to the contour integral along c_4 vanishes provided

$m > -\zeta$. Thus,

$$G_a(i\omega_n^a) = -2\left(\frac{2\pi}{\beta}\right)^{\zeta-1}\tau_0^\zeta \, \text{B}\left(\frac{m+\zeta}{2}, 1-\zeta\right)\begin{cases}\sin\left(\frac{\pi\zeta}{2}\right), & a = b \\ i\cos\left(\frac{\pi\zeta}{2}\right), & a = f\end{cases} \tag{D5}$$

$$G_a(\omega + i\delta) = -\left(\frac{2\pi}{\beta}\right)^{\zeta-1}\tau_0^\zeta \, \text{B}\left(\frac{\zeta}{2} - \frac{i\beta}{2\pi}(\omega+i\delta), \frac{\zeta}{2} + \frac{i\beta}{2\pi}(\omega+i\delta)\right)$$

$$\times \begin{cases}\tan\left(\frac{\pi\zeta}{2}\right)\cosh\left(\frac{\beta\omega}{2}\right) + i\sinh\left(\frac{\beta\omega}{2}\right), & a = b \\ -\cot\left(\frac{\pi\zeta}{2}\right)\sinh\left(\frac{\beta\omega}{2}\right) + i\cosh\left(\frac{\beta\omega}{2}\right), & a = f\end{cases} \tag{D6}$$

$$G_b(\omega + i\delta, \beta \to \infty) \doteq -\frac{\pi\tau_0^\zeta}{\Gamma(\zeta)}\left[\tan\left(\frac{\pi\zeta}{2}\right)|\omega|^{\zeta-1} + i\,\text{sgn}(\omega)|\omega|^{\zeta-1}\right], \tag{D7}$$

$$G_f(\omega + i\delta, , \beta \to \infty) \doteq -\frac{\pi\tau_0^\zeta}{\Gamma(\zeta)}\left[-\cot\left(\frac{\pi\zeta}{2}\right)\text{sgn}(\omega)|\omega|^{\zeta-1} + i|\omega|^{\zeta-1}\right], \tag{D8}$$

where $\text{B}(x,y) = \int_0^\infty dt \, t^{x-1}(1-t)^{y-1}$ is the Euler beta function. In going from Eq. (D5) to (D6) analytical continuation has been performed. Equation (D6) is a function only of the combination $\beta\omega$. In the zero-temperature limit ($\beta \to \infty$), $G_a(\omega)$ displays power-law behavior. Equations (D7) and (D8) are obtained from Eq. (D6) using the relation between the beta and the gamma functions, as well as the asymptotic expansion of the gamma function for $\beta\omega \gg 1$:

$$\Gamma\left(\frac{\zeta}{2} + i\frac{\beta\omega}{2\pi}\right)\Gamma\left(\frac{\zeta}{2} - i\frac{\beta\omega}{2\pi}\right) \doteq 2\pi e^{-\beta\omega/2}\left(\frac{\beta\omega}{2\pi}\right)^{\zeta-1}\Gamma(\zeta),$$

where $\doteq$ indicates the leading-order term. Therefore, the Fourier transform of Eq. (D1) displays ω/T-scaling of the form $T^{\zeta-1}G_a(\omega) = \Phi(\omega/T)$.

If $\zeta \geqslant 1$, the radius τ_0^c of the segments labeled c_2 and c_6 cannot be contracted to zero. As a result, additional terms, controlled by τ_0^c, contribute to the Fourier transform of Eq. (D1).

The case $\zeta = 1$ is realized for the strong coupling fixed point of the standard Kondo model where we identify τ_0^c with $1/T_K$. Indeed, as $T_K \to \infty$, a *trivial* ω/T-scaling is found.

APPENDIX E: SCALING ANSATZ: LEADING AND SUBLEADING BEHAVIOR

In the limit of vanishing temperature $T = 0$, the large-N equations allow for an asymptotically exact solution for $\omega \to 0$. Following Ref. [50], we make the scaling ansatz

$$G_f(\tau, T = 0) = -A_1\left(\frac{\tau_0}{\tau}\right)^{\alpha_f} - A_2\left(\frac{\tau_0}{\tau}\right)^{\alpha_f'} + \cdots, \tag{E1}$$

$$G_B(\tau, T = 0) = -B_1\left(\frac{\tau_0}{\tau}\right)^{\alpha_B} - B_2\left(\frac{\tau_0}{\tau}\right)^{\alpha_B'} + \cdots \tag{E2}$$

for the $T = 0$ solutions of the saddle-point equations at $q = \frac{1}{2}$ with $\alpha_1 < \alpha_2$ and $\beta_1 < \beta_2$. It follows from Eqs. (D8) and (D7) that

$$G_f^{-1}(\omega + i0^+, T = 0) = -\frac{A_1^{-1}}{X_{\alpha_f}^f}\frac{\Gamma(\alpha_f)}{\pi\tau_0^{\alpha_f}}|\omega|^{1-\alpha_f}$$

$$+ \frac{A_2}{A_1^2}\frac{\Gamma(\alpha_f)\Gamma(\alpha_f)}{\Gamma(\alpha_f')}\frac{\tau_0^{\alpha_f'-2\alpha_f}}{\pi}\frac{X_{\alpha_f'}^f}{\left(X_{\alpha_f}^f\right)^2}|\omega|^{1+\alpha_f'-2\alpha_f}, \tag{E3}$$

$$G_B^{-1}(\omega + i0^+, T = 0) = -\frac{B_1^{-1}}{X_{\alpha_B}^B}\frac{\Gamma(\alpha_B)}{\pi\tau_0^{\alpha_B}}|\omega|^{1-\alpha_B} \tag{E4}$$

$$+ \frac{B_2}{B_1^2}\frac{\Gamma(\alpha_B)\Gamma(\alpha_B)}{\Gamma(\alpha_B')}\frac{\tau_0^{\alpha_B'-2\alpha_B}}{\pi}\frac{X_{\alpha_B'}^B}{\left(X_{\alpha_B}^B\right)^2}|\omega|^{1+\alpha_B'-2\alpha_B}, \tag{E5}$$

where $X_\alpha^B = \tan\left(\frac{\pi\alpha}{2}\right) + i\,\text{sgn}(\omega)$ and $X_\alpha^f = -\cot\left(\frac{\pi\alpha}{2}\right)\text{sgn}(\omega) + i$. From the saddle-point equations we obtain for $\Sigma_f(\omega + i0^+, T = 0)$ and $\Sigma_B(\omega + i0^+, T = 0)$ up to and including subleading terms

$$\Sigma_B(\omega) = \frac{\pi A_0 A_1}{\Gamma(\alpha_f)}B(r+1, \alpha_f)X_{r+\alpha_f}^f\tau_0^{r+\alpha_f-1}|\omega|^{r+\alpha_f}\text{sgn}(\omega) + \frac{\pi A_0 A_2}{\Gamma(\alpha_f')}B(r+1, \alpha_f')X_{r+\alpha_f'}^f\tau_0^{r+\alpha_f'-1}|\omega|^{r+\alpha_f'}\text{sgn}(\omega),$$

$$\Sigma_f^1(\omega) = -\frac{\pi\kappa A_0 B_1}{\Gamma(\alpha_B)}B(r+1, \alpha_B)X_{-r-\alpha_B}^B\tau_0^{r+\beta_1-1}|\omega|^{r+\alpha_B}\text{sgn}(\omega) - \frac{\pi\kappa A_0 B_2}{\Gamma(\alpha_B')}B(r+1, \alpha_B')X_{-r-\alpha_B'}^B\tau_0^{r+\alpha_B'-1}|\omega|^{r+\alpha_B'}\text{sgn}(\omega),$$

and

$$\Sigma_f^2(\omega) = -\pi g^2 \frac{K_0^2 A_1}{\Gamma(\alpha_f)} B(2-\epsilon, \alpha_f) X_{\epsilon-\alpha_f-1}^B \tau_0^{\alpha_f-\epsilon} |\omega|^{1+\alpha_f-\epsilon} \text{sgn}(\omega)$$

$$- \pi g^2 \frac{K_0^2 A_2}{\Gamma(\alpha_f')} B(2-\epsilon, \alpha_f') X_{\epsilon-\alpha_f'-1}^B \tau_0^{\alpha_f'-\epsilon} |\omega|^{1+\alpha_f'-\epsilon} \text{sgn}(\omega),$$

which, together with the Dyson equation

$$G_f^{-1}(\omega) = \omega + \lambda - \Sigma_f(\omega), \tag{E6}$$

$$G_B^{-1}(\omega) = J_K^{-1} - \Sigma_B(\omega), \tag{E7}$$

results in a set of conditions for α_f, α_B, α_f', α_B' as well as the leading and subleading amplitudes at the various fixed points (except the trivial one at $J_K = 0$ and $g = 0$). $B(x, y)$ in the self-energy expressions denotes the Euler beta function $B(x, y) = \Gamma(x)\Gamma(y)/\Gamma(x + y)$.

Specifically, we find the following:

(i) The multichannel Kondo and the pseudogap Kondo fixed-point exponents are obtained as solutions of

$$\alpha_f + \alpha_B = 1 - r,$$

$$\kappa = \frac{(1 - \alpha_f) \tan(\pi \alpha_f/2)}{(r + \alpha_f) \tan[\pi (r + \alpha_f)/2]},$$

where the first equation results from equating the leading exponents while the second follows from equating the amplitudes. In a similar fashion, the subleading exponents have to obey
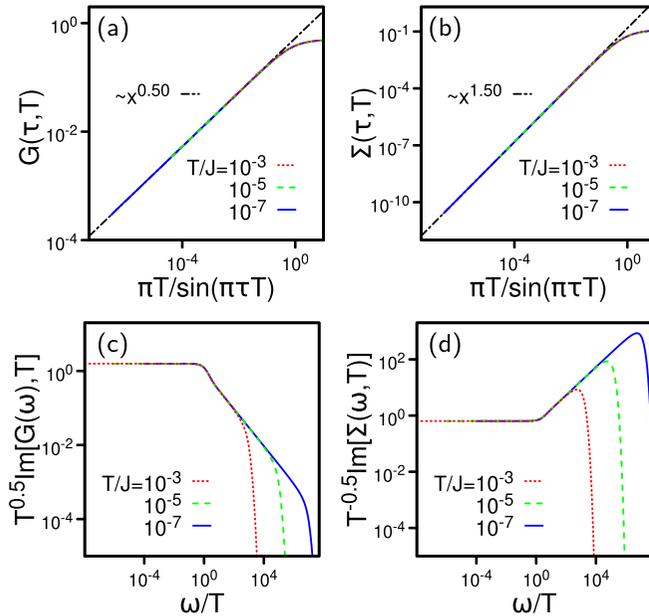
$$\alpha_f' - \alpha_B' + 2\alpha_B = 1 - r$$

$$\times \left(\frac{A_2}{A_1} \frac{\Gamma(\alpha_f)}{\Gamma(\alpha_f')} \right)^2 = \kappa \frac{\pi^2 A_0 A_2 B_2}{\Gamma(\alpha_f')\Gamma(\alpha_B')} B(r+1, \alpha_B')$$

$$\times X_{r+\alpha_B'}^B \left(X_{\alpha_f}^f \right)^2 / X_{\alpha_f'}^f,$$

$$\left(\frac{B_2}{B_1} \frac{\Gamma(\alpha_B)}{\Gamma(\alpha_B')} \right)^2 = \frac{\pi^2 A_0 A_2 B_2}{\Gamma(\alpha_f')\Gamma(\alpha_B')} B(r+1, \alpha_f')$$

$$\times X_{r+\alpha_f'}^f \left(X_{\alpha_B}^B \right)^2 / X_{\alpha_B'}^B.$$

(ii) For the critical point C', one finds for the scaling exponents in leading order $\alpha_f = \epsilon/2$ and $\alpha_B = 1 - r - \epsilon/2$ while the subleading behavior is characterized by $\alpha_f' = \epsilon$ and $\alpha_B' = 1 - r$.

(iii) The leading scaling exponents of the LM$'$ fixed points are $\alpha_f = \epsilon/2$ and $\alpha_B = 1 + r + \epsilon/2$. Likewise, we conclude that the subleading exponents are $\alpha_f' = \epsilon$ and $\alpha_B' = 1 + r + \epsilon$.

In the special case $r = 0$ and $g = 0$, a simple expression for $G_f(\tau)$, valid at any T, has been found to describe our numerical results for $G_f(\tau)$:

$$G_f(\tau) = \left(\frac{A_1^{-1}}{\left(\frac{\pi \tau_0/\beta}{\sin(\pi \tau/\beta)} \right)^{\alpha_f}} + \frac{1}{q_0} \right)^{-1}, \tag{E8}$$

which is in line with the results of Ref. [50]. Figure 14 shows a comparison of Eq. (E8) with the numerical solution of the large-N equations for the particle-hole-symmetric case, i.e., $q_0 = \frac{1}{2}$. For $G_B(\tau)$, no equivalent expression valid at all τ and T has been found.

FIG. 15. Numerical solution of (a) $G(\tau)$ and (b) $\Sigma(\tau)$ at different temperature. ω/T-scaling of Im$G(\omega)$ and Im$\Sigma(\omega)$ at different temperature.
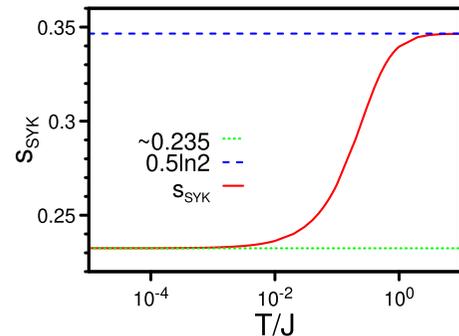

FIG. 16. Temperature dependence of the entropy of the SYK model. Our result interpolates between the analytical known results for $s_{\text{SYK}}(T = 0)$ and $s_{\text{SYK}}(T \gg J)$.

APPENDIX F: SCALING AND ENTROPY IN THE SYK MODEL

The large-N equation of the SYK model is

$$\Sigma(\tau) = -J^2 G(-\tau)^3, \tag{F1}$$

together with the Dyson equation

$$G(i\omega_n) = \frac{1}{i\omega_n - \Sigma(i\omega_n)}, \tag{F2}$$

where $i\omega_n$ ($n = \pm 1, \pm 3, \dots$) are fermionic Matsubara frequencies and J is a coupling constant. The strong coupling limit of the SYK model is known to possess an emergent conformal invariance and the $T = 0$ residual entropy has been obtained using analytic methods. One can also show that the entropy approaches $1/2 \ln 2$ at high T [67]. From the Luttinger-Ward functional,

$$F = \frac{-T}{2} \ln 2 + \frac{1}{2\pi} \int d\omega \, f(\omega) \left\{ \text{Im} \left[\ln \left(\frac{-G(\omega)^{-1}}{-G_0(\omega)^{-1}} \right) \right] \right.$$
$$\left. + \text{Im}[\Sigma(\omega) G(\omega)] - \frac{J^2}{4} \int_\tau G(\tau)^4 \right\}, \tag{F3}$$

the entropy follows as

$$s_{\text{SYK}} = \frac{1}{2} \ln 2 - \frac{1}{2\pi} \int d\omega \frac{df(\omega)}{dT} \left\{ \text{Im} \ln \left[\frac{G_0(\omega)}{G(\omega)} \right] \right.$$
$$\left. + \text{Im}[\Sigma(\omega)] \text{Re}[G(\omega)] \right\}. \tag{F4}$$

Applying the scaling ansatz

$$G(\tau) = -A \left(\frac{\tau_0}{\tau} \right)^\alpha - B \left(\frac{\tau_0}{\tau} \right)^{\alpha'} \tag{F5}$$

to the SYK model yields $\alpha = 0.5$ and $\alpha' = 2\alpha$. We solve the self-consistent equation in real frequency space and obtain $G(\omega)$, $G(\tau)$ as well as the entropy $s_{\text{SYK}}(T)$. The resulting scaling properties of $G(\tau)$, $\Sigma(\tau)$ and the complementary ω/T-scaling of $G(\omega)$ and $\Sigma(\omega)$ are shown in Fig. 15. The entropy $s_{\text{SYK}}(T)$, shown in Fig. 16, flows from the weak coupling fixed point at high T, to the strong coupling fixed point at $T = 0$. Our results for $s_{\text{SYK}}(T)$ and the exponents ($\alpha = \frac{2}{q} = 0.5$) for $G(\omega)$ and $G(\tau)$ agree well with analytical prediction [67].

[1] J. Hertz, Phys. Rev. B **14**, 1165 (1976).

[2] S. Sachdev, *Quantum Phase Transitions* (Cambridge University Press, Cambridge, 1999).

[3] N. E. Hussey, H. Gordon-Moys, J. Kokalj, and R. H. McKenzie, J. Phys. Conf. Ser. **449**, 012004 (2013).

[4] B. Keimer, S. A. Kivelson, M. R. Norman, S. Uchida, and J. Zaanen, Nature (London) **518**, 179 (2015).

[5] Q. Si, S. Rabello, K. Ingersent, and J. L. Smith, Nature (London) **413**, 804 (2001).

[6] P. Coleman, C. Pépin, Q. Si, and R. Ramazashvili, J. Phys.: Condens. Matter **13**, R723 (2001).

[7] Q. Si, Phys. B (Amsterdam) **378-380**, 23 (2006).

[8] P. Coleman and A. H. Nevidomskyy, J. Low Temp. Phys. **161**, 182 (2010).

[9] Q. Si, J. H. Pixley, E. Nica, S. J. Yamamoto, P. Goswami, R. Yu, and S. Kirchner, J. Phys. Soc. Jpn. **83**, 061005 (2014).

[10] S. Kirchner, S. Paschen, Q. Chen, S. Wirth, D. Feng, J. D. Thompson, and Q. Si, Rev. Mod. Phys. **92**, 011002 (2020).

[11] T. Park, V. A. Sidorov, F. Ronning, J.-X. Zhu, Y. Tokiwa, H. Lee, E. D. Bauer, R. Movshovich, J. L. Sarrao, and J. D. Thompson, Nature (London) **456**, 366 (2008).

[12] K. Grube, S. Zaum, O. Stockert, Q. Si, and H. v. Löhneysen, Nat. Phys. **13**, 742 (2017).

[13] B. Wolf, Y. Tsui, D. Jaiswal-Nagar, U. Tutsch, A. Honecker, K. Remović-Langer, G. Hofmann, A. Prokofiev, W. Assmus, G. Donath, and M. Lang, Proc. Natl. Acad. Sci. U. S. A. **108**, 6862 (2011).

[14] P. Noziéres and A. Blandin, J. Phys. **41**, 193 (1980).

[15] A. M. Tsvelick, J. Phys. C: Solid State Phys. **18**, 159 (1985).

[16] S. Kirchner, Adv. Quantum Technol. **3**, 1900128 (2020).

[17] D. Withoff and E. Fradkin, Phys. Rev. Lett. **64**, 1835 (1990).

[18] C. Gonzalez-Buxton and K. Ingersent, Phys. Rev. B **57**, 14254 (1998).

[19] K. Ingersent and Q. Si, Phys. Rev. Lett. **89**, 076403 (2002).

[20] L. Fritz, S. Florens, and M. Vojta, Phys. Rev. B **74**, 144410 (2006).

[21] M. Vojta, Phys. Rev. Lett. **87**, 097202 (2001).

[22] M. T. Glossop and D. E. Logan, Europhys. Lett. **61**, 810 (2003).

[23] M. T. Glossop, G. E. Jones, and D. E. Logan, J. Phys. Chem. B **109**, 6564 (2005).

[24] M. T. Glossop, S. Kirchner, J. H. Pixley, and Q. Si, Phys. Rev. Lett. **107**, 076404 (2011).

[25] J. H. Pixley, S. Kirchner, K. Ingersent, and Q. Si, Phys. Rev. Lett. **109**, 086403 (2012).

[26] L. G. G. V. Dias da Silva, N. P. Sandler, K. Ingersent, and S. E. Ulloa, Phys. Rev. Lett. **97**, 096603 (2006).

[27] A. Zhuravlev, I. Zharekeshev, E. Gorelov, A. I. Lichtenstein, E. R. Mucciolo, and S. Kettemann, Phys. Rev. Lett. **99**, 247202 (2007).

[28] Q. Si and J. L. Smith, Phys. Rev. Lett. **77**, 3391 (1996).

[29] Q. Si, J. L. Smith, and K. Ingersent, Int. J. Mod. Phys. B **13**, 2331 (1999).

[30] A. M. Sengupta, Phys. Rev. B **61**, 4041 (2000).

[31] T. Senthil, M. Vojta, and S. Sachdev, Phys. Rev. B **69**, 035111 (2004).

[32] S. Paschen, T. Lühmann, S. Wirth, P. Gegenwart, O. Trovarelli, C. Geibel, F. Steglich, P. Coleman, and Q. Si, Nature (London) **432**, 881 (2004).

[33] S. Friedemann, N. Oeschler, S. Wirth, C. Krellner, C. Geibel, F. Steglich, S. Paschen, S. Kirchner, and Q. Si, Proc. Natl. Acad. Sci. U. S. A. **107**, 14547 (2010).

[34] S. Friedemann, S. Wirth, S. Kirchner, Q. Si, S. Hartmann, C. Krellner, C. Geibel, T. Westerkamp, M. Brando, and F. Steglich, J. Phys. Soc. Jpn. **80**, SA002 (2011).

[35] L. Prochaska, X. Li, D. C. MacFarland, A. M. Andrews, M. Bonta, E. F. Bianco, S. Yazdi, W. Schrenk, H. Detz, A. Limbeck, Q. Si, E. Ringe, G. Strasser, J. Kono, and S. Paschen, Science **367**, 285 (2020).

[36] A. J. Millis, Phys. Rev. B **48**, 7183 (1993).

[37] L. Zhu, S. Kirchner, Q. Si, and A. Georges, Phys. Rev. Lett. **93**, 267201 (2004).

[38] A. Cai, Z. Yu, H. Hu, S. Kirchner, and Q. Si, Phys. Rev. Lett. **124**, 027205 (2020).

[39] L. Zhu and Q. Si, Phys. Rev. B **66**, 024426 (2002).

[40] G. Zaránd and E. Demler, Phys. Rev. B **66**, 024427 (2002).

[41] R. Bulla, N.-H. Tong, and M. Vojta, Phys. Rev. Lett. **91**, 170601 (2003).

[42] M. T. Glossop and K. Ingersent, Phys. Rev. Lett. **95**, 067202 (2005).

[43] S. Kirchner, L. Zhu, Q. Si, and D. Natelson, Proc. Natl. Acad. Sci. U. S. A. **102**, 18824 (2005).

[44] F. Zamani, P. Ribeiro, and S. Kirchner, New J. Phys. **18**, 063024 (2016).

[45] M. Vojta and M. Kirćan, Phys. Rev. Lett. **90**, 157203 (2003).

[46] M. Kirćan and M. Vojta, Phys. Rev. B **69**, 174421 (2004).

[47] M. Glossop, N. Khoshkhou, and K. Ingersent, Phys. B (Amsterdam) **403**, 1303 (2008).

[48] J. H. Pixley, S. Kirchner, K. Ingersent, and Q. Si, Phys. Rev. B **88**, 245111 (2013).

[49] J. H. Pixley, S. Kirchner, M. T. Glossop, and Q. Si, J. Phys. Conf. Ser. **273**, 012050 (2011).

[50] O. Parcollet, A. Georges, G. Kotliar, and A. Sengupta, Phys. Rev. B **58**, 3794 (1998).

[51] D. L. Cox and A. E. Ruckenstein, Phys. Rev. Lett. **71**, 1613 (1993).

[52] F. Zamani, T. Chowdhury, P. Ribeiro, K. Ingersent, and S. Kirchner, Phys. Status Solidi B **250**, 547 (2013).

[53] I. Affleck and A. W. W. Ludwig, Phys. Rev. Lett. **67**, 161 (1991).

[54] J. L. Cardy, Nucl. Phys. B **240**, 514 (1984).

[55] P. Ginsparg, in *Fields, Strings and Critical Phenomena*, edited by E. Brézin and J. Zinn-Justin, Les Houches, Session XLIX, 1989 (North-Holland, Amsterdam, 1990).

[56] D. Friedan and A. Konechny, Phys. Rev. Lett. **93**, 030402 (2004).

[57] S. Kirchner and Q. Si, Phys. Rev. Lett. **100**, 026403 (2008).

[58] A. K. Mitchell, M. Vojta, R. Bulla, and L. Fritz, Phys. Rev. B **88**, 195119 (2013).

[59] M. Cheng, T. Chowdhury, A. Mohammed, and K. Ingersent, Phys. Rev. B **96**, 045103 (2017).

[60] P. Ribeiro, F. Zamani, and S. Kirchner, Phys. Rev. Lett. **115**, 220602 (2015).

[61] G. Baym and L. P. Kadanoff, Phys. Rev. **124**, 287 (1961).

[62] P. Coleman, I. Paul, and J. Rech, Phys. Rev. B **72**, 094430 (2005).

[63] J. Rech, P. Coleman, G. Zarand, and O. Parcollet, Phys. Rev. Lett. **96**, 016601 (2006).

[64] M. Potthoff, Condens. Matter Phys. **9**, 557 (2006).

[65] R. Bulla, T. Pruschke, and A. C. Hewson, J. Condens. Matter Phys. **9**, 10463 (1997).

[66] R. Žitko, Phys. Rev. B **80**, 125125 (2009).

[67] J. Maldacena and D. Stanford, Phys. Rev. D **94**, 106002 (2016).

[68] S. Florens and A. Rosch, Phys. Rev. Lett. **92**, 216601 (2004).

[69] J. Zinn-Justin (private communication).

[70] J. Dai, Q. Si, and C. J. Bolech, arXiv:0712.3280.

[71] H. Casini, I. S. Landea, and G. Torroba, J. High Energy Phys. 10 (2016) 140.

[72] J. H. Pixley, T. Chowdhury, M. T. Miecnikowski, J. Stephens, C. Wagner, and K. Ingersent, Phys. Rev. B **91**, 245122 (2015).

[73] E. Lebanon, J. Rech, P. Coleman, and O. Parcollet, Phys. Rev. Lett. **97**, 106604 (2006).